Geostatistical modeling of Rock Quality Designation (RQD) and geotechnical zoning accounting for directional dependence and scale effect

L. Katherine Sánchez, Xavier Emery, Serge Antoine Séguret

Geostatistical modeling of Rock Quality Designation (RQD) and geotechnical zoning accounting for directional dependence and scale effect

L. Katherine Sánchez [a,b,c,d,*, 1], Xavier Emery [a,b, 2], Serge A. Séguret [d, 3]

[a] Advanced Mining Technology Center, University of Chile, Santiago, Chile
[b] Department of Mining Engineering, University of Chile, Santiago, Chile
[c] CSIRO-Chile International Center of Excellence in Mining and Mineral Processing, Santiago, Chile
[d] Centre de Géosciences, MINES ParisTech, PSL University, Paris, France
* Corresponding author: katherine.sanchezc@ug.uchile.cl; katherine.sanchez@mines-paristech.fr

Abstract

The characterization of rock masses is an essential component for the planning and development of engineering designs in rock mechanics and rock engineering. The Rock Quality Designation (RQD) is a widely used rock mass characterization system that is direction-dependent, i.e., the measurement of a core sample depends not only on the sample position but also on its orientation. This paper outlines the critical aspects of the determination of RQD and proposes a physically-based upscaling strategy from borehole samples to large blocks, based on block-averaging the RQD values corresponding to the same direction, then calculating the minimum value over all the directions. An anisotropy index indicating how much RQD varies between one direction and another is also derived. Using geostatistical simulation, our proposal allows interpolating and upscaling direction-dependent geotechnical variables like RQD at any place in the geographical space for any

[1] L. Katherine Sánchez: Investigation; Formal analysis; Writing - Original Draft; Visualization.
[2] Xavier Emery: Conceptualization; Methodology; Resources; Writing - Review & Editing; Supervision
[3] Serge A. Séguret: Conceptualization; Methodology; Writing - Review; Supervision.

direction, avoiding directional biases. We illustrate this proposal by predicting RQD in a polymetallic deposit, achieving geotechnical zoning and comparing the results with those of the traditional approach where the directional dependence of RQD is ignored.

Keywords: RQD; geostatistical simulation; geotechnical zoning; directional dependence; upscaling.

1. Introduction

Proper zoning or domaining of areas presenting similarities in the lithological, structural, hydrogeological and rock quality components is of utmost importance for successful geotechnical designs in mining, geological and geotechnical engineering. The strength and deformability parameters of rock masses and the nature of the discontinuity network constitute complex information whose incorporation into the definition of different geotechnical domains is challenging and still a subject of significant uncertainties (Barton, 1990; Hudson, 2012; Chowdhury et al., 2012) that do not evade to the well-known RQD (Rock Quality Designation; Deere et al., 1967) classification system.

The RQD values are sensitive to the direction in which the core sample is collected (Palmström, 1982; Elsayed and Sen, 1991; Choi and Park, 2004; Emery and Séguret, 2020) and cannot be extrapolated straightforwardly to a more voluminous support, e.g., a three-dimensional block or the entire rock mass (Hoek and Brown,1980; Sen and Kazi, 1984; Cunha, 1990) without a proper management of the directional nature of the measurements. The directional dependence and the change of volumetric support (upscaling) are two critical aspects overlooked today by many practitioners, preventing a correct understanding of the spatial behavior of the rock mass and leading to inaccurate predictions.

The widely accepted practice of scaling the mechanical properties from a small piece of rock (e.g., a cylindrical borehole core, idealized as a 'line' support) to a three-dimensional 'block' support implies an assumption of isotropy (i.e., no directional dependence) of these properties at the working scale. Nevertheless, the geological materials often present spatial heterogeneities exhibiting a high contrast of the mechanical properties measured at two different locations, even at small distances (e.g., Cai, 2011; Song et al., 2011; Matonti et al., 2015; Pinheiro et al., 2016; Vatcher et al., 2016; Gao et al., 2018). Such a contrast may also vary with the relative angle between the measurements, being less when comparing two parallel borehole cores than when comparing two perpendicular cores. The integration of these subsurface variabilities into models to simulate the behavior of the rock masses would be theoretically the right way to go. Therefore, the predictive reliability of any model applied to rock engineering is strongly dependent on an accurate representation of the spatial and directional variability of the modeled variable(s). In this context, we propose to use a geostatistical model taking account of the directional sensitiveness of RQD to facilitate the upscaling from line-supports to block-supports and to obtain a better representation of the degree of jointing or fracturing of rock masses.

Geostatistical tools allow integrating spatial variability into the modeling of the rock mass. The application of geostatistics in geotechnics is not a new topic (e.g., Oh et al., 2004; Stavropoulou et al., 2007; Exadaktylos and Stavropoulou, 2008; Choi et al., 2009; Ferrari et al., 2014; Pinheiro et al., 2016; Chen et al., 2017; Hekmatnejad et al., 2017; Boyd et al., 2019). However, the traditional geostatistical modeling applied to RQD for characterizing rock masses (Ozturk and Nasuf, 2002; Ozturk and Simdi, 2014; Madani and Asghari, 2013) only considers its variability in the three-dimensional geographical space, disregarding its directional dependence, e.g., when there is a predominant joint set, such as foliation and schistosity joints in metamorphic rocks. This work aims to compare the traditional approach (ignoring directional dependence) with a new proposed approach considering the directional

dependence of RQD, illustrated with a case study of a polymetallic deposit. The results will highlight the advantages of the latter approach in the geotechnical zoning, knowledge of the spatial behavior of rock masses, and management of uncertainties in underground projects. The background and details of the proposed methodology are explained in Sections 2 and 3 and Appendix A, whereas the case study is presented in Section 4. A discussion, conclusions, and perspectives for future work follow in Sections 5 and 6.

2. Background: directional dependence and upscaling of RQD

The RQD rating (Deere et al., 1967) provides a quantitative measure of the degree of jointing or fracturing of rock mass from boreholes, consisting of 100 times the ratio between the total length of core pieces larger than 100 millimeters and the total core run length. The RQD classification system uses a continuous scale ranging from 0 to 100 to assign the rock mass quality and position it within one of five classes (excellent, good, fair, poor, very poor). In addition to the direct RQD calculation method, indirect methods have also been developed to estimate RQD considering different input data (Priest and Hudson, 1976; Palmström, 1982, 2005; Zheng et al., 2018) and to incorporate it into rock classification schemes (Bieniawski, 1973; Barton et al., 1974; Hoek et al., 2013). However, already since its conception, there is an awareness of one of its most obvious shortcomings: its directional dependence (e.g., Deere, 1989; Choi and Park, 2004). In the following, the directional dependence and upscaling will be described, providing details on how previous researchers have tackled them and how we will deal with them in our geostatistical model.

2.1 Directional dependence

The RQD values vary in space and according to the angle between the direction of the sample (borehole or scanline) and the discontinuities present in a rock mass. Since this

105 directional dependence cannot be fixed, it is impossible to directly assess joint spacing
106 conditions unless they do not depend on the direction (isotropic discontinuity network, whose
107 properties are invariant under a rotation). Some attempts to minimize the biases caused by
108 the directional dependence focused on drilling as many boreholes with different directions as
109 possible (Deere, 1989), modifying the original RQD concept, such as estimating RQD from
110 the volumetric joint count J_v (Palmström, 2005), considering Terzaghi's correction and a
111 fractured zone effect (Haftani et al., 2016), or performing the calculation based on weak
112 zones (core washed, crushed zones, karst cavities) and joint orientation (Azimian, 2016).
113 However, an alternative definition of RQD is unknown to most engineers, practitioners, and
114 researchers. Moreover, these new RQD conceptualizations lose their most potent and
115 engaging property: simplicity. On the other hand, cost-efficiency and other practical
116 considerations limit the number of boreholes drilled for an underground exploratory
117 campaign.
118
119 An alternative solution to deal with RQD directional dependence has been proposed
120 by Séguret and Guajardo (2015), who classified the borehole samples according to their
121 sampling directions. However, this proposal does not circumvent all the limitations since
122 RQD values can be predicted only in the directions that have been drilled, lacking any proper
123 interpolation between them. Recently, Zheng et al. (2018) provide a new perspective about
124 the directional dependence of RQD, considering this property as an advantage and
125 proposing to estimate an anisotropy index of the jointing degree. The latter authors suggest
126 selecting the minimum RQD value and its corresponding direction as the most representative
127 of a specific rock mass, which potentially reflects its real jointing degree and directly
128 compares with other rock masses. However, this approach only applies to scanlines (in
129 outcrops or excavation faces) with different orientations for the same location, in relatively
130 intact rock masses (from medium weathered to fresh hard), and statistically homogeneous
131 regions. Except for the case of an isotropic discontinuity network, the selection of a

representative direction (here, the one corresponding to the minimum RQD) implies a loss of information on the directional behavior of RQD.

We build on the best of each previous attempt to propose an alternative solution that considers the real regionalization space of RQD as the usual geographical 3D space crossed by the 2D space of dip and azimuth. Specifically, the RQD for one composite sample depends on the geographical position $\boldsymbol{x}$ (x_1, y_1, z_1) of its gravity center and the direction $\boldsymbol{u}$ (α, ϕ) of the sample, with **u** a point of the unit sphere $\mathbb{S}^2$ of $\mathbb{R}^3$ characterized by its azimuth α and dip ϕ, see Fig. 1 and Appendix A. This approach leads to the RQD measurements being assigned to five coordinates, which will allow evaluating the correlation between RQD values observed at different locations of this five-dimensional space (thus, depending not only on the geographical coordinates of the measurements but also on their angular coordinates).

2.2 Upscaling

The dependence of the mechanical properties of a rock mass with the geometric dimensions of the sample is known as the scale or support effect (Bieniawski, 1968; Pratt et al., 1972; Bandis et al., 1981; Barton, 1990; Cunha, 1990; Cuisiat and Haimson, 1992). This effect is a potential drawback for the spatial interpolation of mechanical properties observed at a limited (in size) sample to the overall rock mass. Considering that RQD in line supports (at borehole core or scanline scale) has a directional dependence, this dependence should remain in any subsequent change of support. In particular, such a change of support should not mix RQD values measured along different directions unless the discontinuity network in the rock mass is isotropic, in which case directional dependence does not arise.

In practice, the support effect can be overlooked when a particular rock mass consists of purely intact rock or individual jointed block pieces are too small compared to the overall

158 size of the engineering structure being considered. Hoek and Brown's criterion can thus be
159 applied at the excavation/pit scale (Edelbro, 2004, Marinos and Carter, 2018). In such a
160 situation, rock masses can be assumed as a continuum and isotropic medium, and the
161 calculation of arithmetic averages from boreholes or scanlines (line-supports) to rock mass
162 (block-supports) is justifiable (Marinos et al., 2005; Hoek, 2006). Then, when comparing the
163 construction scale of rock excavations with the block size of intact rock, one can assume the
164 rock mass is closely jointed and be treated as a homogeneous continuous equivalent whose
165 discontinuities are implicit. However, such an assumption is not always possible and rarely
166 occurs due to the nature of geological materials affected by tectonism, weathering, and
167 alteration processes.
168
169 Our approach to addressing the support effect is twofold. On the one hand, it is
170 proposed to define a direction-dependent upscaled RQD value in a given block by averaging
171 the RQD values measured along the same direction at different points discretizing the block,
172 without mixing values measured in different directions. In this way, it is possible to know the
173 directional variability of RQD in each block, accounting for the anisotropy of the rock mass
174 and giving insights into the geometry of the fragments formed by the intersection of joints in a
175 rock mass. On the other hand, in addition to this 'directional' block-support RQD, we will also
176 propose a 'non-directional' block-support RQD by selecting the minimum RQD value (not the
177 average) across all the directions of the two-dimensional angular space represented by a unit
178 sphere, which is deemed the most representative value of the real jointing degree of the
179 block. Accordingly, the 'directional' block-support RQD will be regionalized in the five-
180 dimensional (geographical × angular) space, as is the RQD measured on core samples,
181 while the 'non-directional' one will be regionalized only in the 3D geographical space.

182 ## 3. Methodology: geostatistical modeling and simulation

183

Since it is defined on a continuous quantitative scale, RQD can be transformed into a variable (hereafter, denoted as Z) with a standard Gaussian distribution, a process known as Gaussian anamorphosis or normal-scores transformation (Chilès and Delfiner, 2012). Such a transformation is the first stage for geostatistical modeling, where the transformed variable (Z) is viewed as a Gaussian random field. In practice, the characterization of such a random field reduces to that of its mean value (here, the mean is set to zero) and its autocovariance function or, equivalently, its variogram.

To simulate RQD, the following steps should be accomplished (details in Appendix A):

I. The original RQD data are transformed into Gaussian data (normal scores), and an anamorphosis function that maps the RQD data into normal scores is defined.

II. A variogram analysis of the normal scores data is performed, consisting in computing an experimental variogram that measures half the variance of the increment between two measurements based on their geographical and angular separations when RQD is regionalized in a 5D space or just on their geographical separation when RQD is regionalized in the 3D space. Subsequently, the experimental variogram is fitted with a theoretical model.

III. A Gaussian random field is simulated at all the target locations and conditioned to the available data. The latter implies that the simulated values at locations with data must coincide with the data values. Here, we use the turning bands algorithm (Matheron, 1973) for the random field simulation and a post-processing kriging (Chilès and Delfiner, 2012) for conditioning the simulated outcomes to the sampling data.

IV. The Gaussian simulation is back-transformed to the RQD original scale by using the anamorphosis function defined at step I.

4. Case study: jointed rock mass in a polymetallic deposit

To illustrate the proposed methodology and compare it with the traditional approach, we present a case study corresponding to an underground mining operation. The aims are to simulate RQD within the deposit, considering its directional dependence and a change of support that can adequately characterize a volumetric support and be used for geotechnical zoning.

4.1. Geological setting and data preparation

The case study corresponds to a polymetallic deposit, the name and location of which will not be disclosed for confidentiality reasons. In an irregular tubular body, the mineralization is of the distal skarn type, related to intrusives of intermediate composition, where the most frequent alterations are chloritization and skarn type. The ore zone mainly comprises skarn and limestones.

The deposit is located along a deformed belt composed of back-arc siliciclastic and carbonates rocks, unconformably covered with volcanic rocks, intruded by intermediate granodiorite and quartz-monzonite stocks and sills, the emplacement of which is structurally controlled by north-to-south-oriented faults. The structural evolution involves compressional reactivation of pre-existing extensional faults and strike-slip episodes of deformation. Two main structural domains have been identified: an ENE-vergent fold-and-thrust system with steep dip angles (75° SE), while the second one is linked to dextral strike-slip movements with variable strikes and steep dips angles (60-80° SE). The discontinuities identified from geotechnical boreholes can be grouped into three main families, two sub-vertical and one sub-horizontal, the orientations of which corroborate the influence of the regional structural

234 background at the ore deposit scale rock mass (Fig. 2). Locally, sub-vertical and mid-dip
235 secondary discontinuity systems also arise.
236
237 The rock mass is stratified with a moderate weathering, the spacing of the strata
238 being between 6 and 20 cm, with a persistence greater than 20 m, opening less than 1 mm
239 without filling, except for a slime patina. The metamorphosed limestone rock mass is more
240 competent than rocks of similar composition, but is more brittle, with a higher Hoek-Brown
241 modulus value (mi = 14) compared with their unmetamorphosed parent carbonate rocks (mi
242 = 12). The ore zone and its environment have rock mass qualities that generally range from
243 fair to good (RMR between 50 and 75), except for localized fault zones where the rock mass
244 quality is poor (RMR between 25 and 35). The water condition is humid and adversely
245 influences the stability of the underground excavations, and can vary to wet due to water
246 seepage in fault areas.
247
248 Boreholes have been drilled from the surface and from underground galleries, along
249 which geologists have measured RQD and other geotechnical variables on intervals of
250 lengths varying between 1 and 4 m. To model RQD, we calculated average values for 3 m
251 long composites along the boreholes. The resulting database contains 3800 composited data
252 with their locations (easting, northing, elevation, azimuth, dip) and rock quality designations.
253 The sampled volume is about 350 × 500 × 700 m^3.

254 *4.2. RQD modeling*

255
256 As the distribution of RQD differs significantly from a Gaussian distribution (Fig. 3), a
257 normal score transformation (anamorphosis) is performed before variogram analysis and
258 simulation. The transformation accounts for declustering weights calculated with the cell

method (Journel, 1983), giving more importance to isolated data and downweighting clustered data to correct the effects caused by the irregularities of the sampling mesh.

We performed variogram calculations according to the parameters listed in Table 1 to identify preferential directions of continuity in the geographical space. The calculated variograms (Fig. 4) show that no significant anisotropy in the geographical space exists for the normal scores data, be they regionalized in the 3D or the 5D space. The latter owes to experimental variograms calculated along different directions of the 3D space (with a fixed angular separation between paired data in the 5D approach) overlap to a great extent. Thus, henceforth, only omnidirectional variograms are calculated in the geographical space (Fig. 5). The discontinuity observed at the origin ('nugget effect') is interpreted as a consequence of the small-scale variability of RQD, where continuity is not perceptible. On the other hand, it is also seen that the experimental variogram increases with the geographical separation distance and with the angular separation of the paired data until it reaches a sill at geographical separations of about 60 to 100 m. The better continuity of RQD (slower increase and lower sill) occurs when the angular separation between the measurements is low.

These experimental variograms of the 5D regionalized data are fitted by basic nesting models, each being the product of two components: a stationary geographical correlation and an isotropic angular correlation. The fitted variogram model is the following:

$$\gamma_{RQD}(\boldsymbol{h},\delta) = (0.19)nugget(\boldsymbol{h}) + (0.20)sph_{20,0}(\boldsymbol{h},\delta) + (0.35)sph_{40,0}(\boldsymbol{h},\delta) + (0.14)sph_{130,0}(\boldsymbol{h},\delta) + (0.10)sph_{130,2}(\boldsymbol{h},\delta) + (0.14)sph_{\infty,2}(\boldsymbol{h},\delta)$$

with $\boldsymbol{h}$ and δ being the geographical and angular separations between two measurements (Fig. 4e), and $sphL_{a,n}(\boldsymbol{h},\delta)$ being one minus the product of an isotropic spherical correlation

with a range *a* evaluated at ***h,*** and a Legendre polynomial of degree *n* evaluated at cos(δ), see Eq. (A.4) in Appendix A.

The variogram model for the 5D regionalized data fits quite well the calculated experimental points for all the different geographical and angular separations between paired data (Fig. 5). The first milestone on the ordinate axis corresponds to the nugget effect, with a partial sill of 0.19. After that, one uses three nested structures corresponding to the product of a spherical covariance with a range of 20, 40, or 130 m and a zero-degree Legendre polynomial. The latter is identically equal to 1, so that the three nested structures exclusively depend on the geographical separation. Finally, two nested structures consider the product of long-range spherical covariances with a second-degree Legendre polynomial, varying with the angular separation. The use of a zonal anisotropy (spherical structure with an infinite range) and the fact that the second-degree Legendre polynomial changes from positive to negative values as the angular separation increases allow modeling the increase in the variogram sill with the angular separation.

For the traditional approach (3D regionalized data), we consider only the basic nested structures that depend on the geographical coordinates, and the variogram model remains as follows:

$$\gamma_{RQD}(\boldsymbol{h}) = (0.19)nugget(\boldsymbol{h}) + (0.20)sph_{20,0}(\boldsymbol{h}) + (0.35)sph_{40,0}(\boldsymbol{h}) + (0.24)sph_{130,0}(\boldsymbol{h})$$

The proposed variogram models (for both the traditional and directional approaches) are validated using leave-one-out cross-validation techniques (Fig. 6). The RQD at each data location is simulated 500 times conditionally to the neighboring data in a radius of 200 m, excluding the five adjacent composites from either side of the same borehole to avoid considering data too close to the target location. The outcomes of the 500 simulations are

313 then averaged to obtain a prediction at the data location, which is compared against the true
314 RQD value. The dispersion diagram between predicted and true RQD values for both
315 approaches has a regression line that matches the first bisector (Figs. 6a, c), proving that the
316 simulations are conditionally unbiased (Chilès and Delfiner, 2012). Furthermore, accuracy
317 plots (Goovaerts, 2001) allow evaluating the capability of the 500 simulations to measure the
318 uncertainty associated with the true values: the fraction of true values belonging to the *p*-
319 probability interval is practically equal to *p*, whatever this probability is in [0,1] (Figs. 6b, d).

320 *4.3. Conditional simulation*

321

322 Simulation is performed in the geographical space on a regular grid with a mesh of 2
323 m x 2 m x 20 m covering part of the sampled region, for three directions in the angular space:
324 north, east and vertical. Five hundred simulations of RQD are constructed at each target grid
325 node and direction. The maps plotted in Figs. 7 and 8 show a horizontal slice (43,750 nodes)
326 at elevation 350 m above the mean sea level of the geographical space. The borehole data
327 distant less than 10 m from the target grid (Fig. 7) or less than 10 m from the target grid and
328 45° from the target direction (Fig. 8) are superimposed, together with envelopes delimitating
329 'confidence regions' inside which the kriging error variance is less than 90% of the data
330 variance (i.e., the borehole data are informative and significantly reduce the uncertainty
331 inside the envelope). In the maps of the average of the 500 simulations, the most remarkable
332 contrast in RQD is observed in areas where the borehole data are present for both the
333 traditional (Fig. 7b) and directional (Figs. 8b, d, f) approaches. This contrast is consistent with
334 field information, according to which the rock mass quality is good (RQD > 75) in the eastern
335 side of the sampled area, corresponding to the ore zone, and becomes regular (RQD < 50) in
336 the western side.

337

For both approaches, the simulated RQD values vary from a poor (RQD ~40%) to an excellent (RQD >90%) rock quality in just a few tens of meters apart (Figs. 7a, 8a, 8c, 8e). The map for the average of the 500 simulations using the traditional approach (Fig. 7b) shows a more significant similarity with the average map of the directional approach when RQD is simulated along the north direction (Fig. 8b). This coincidence is an artifact since most of the boreholes in the study area are oriented sub-horizontally and mainly in a north-southeast direction, as corroborated by the superimposed borehole data on the maps.

Geologists and mining engineers could interpret very favorable conditions towards the east of the study area only based on Fig. 7b (traditional approach), corroborating the influence of the major structural domains (ENE-vergent fold-and-thrust system with dip angle 75° SE, and dextral strike-slip movements with dips angles 60-80° SE). Even though it is true that a better rock quality is present in that sub-area, this interpretation is conditioned by the RQD values measured along a specific sampling direction, which is likely to be biased with respect to the RQD measured in other directions for the same area. The risk of bias is minimized when RQD is simulated along different directions using the directional approach, and one can be aware of the variations of RQD in the geographical space and the angular space. The good rock quality towards the east, evidenced in all the maps, above all along the vertical and north directions (Figs. 8b, d, f), can be confidently interpreted as the real behavior of the rock mass. The comparison between the simulation results in the absence or presence of a directional component allows visualizing the spatial variability to be expected in the field for a given direction. The latter is helpful in quantitatively define favorable conditions for the advance of the excavation from a quantitatively and non-qualitatively point of view, as is currently done in Bieniaswski's RMR classification.

4.4. Change of support (upscaling)

364 The change from the sample support (cylindrical borehole composite) to block
365 support implies averaging simulated RQD values in the geographical space. However, it
366 does not make sense to average RQD values associated with different directions. For the
367 change of support to be meaningful, a single direction has to be chosen, and all the RQD
368 values being averaged should correspond to this direction. In the traditional approach, the
369 selection of an appropriate direction to conduct a change of support is a challenge, insofar as
370 it is necessary to find a 'representative' direction for (a) measuring RQD and (b) averaging
371 the RQD values on the block: otherwise, one calculates a non-directional block-support RQD
372 value that mixes different directions (Fig. 9, right panel). In the proposed (directional)
373 approach, the problem is solved straightforwardly by defining as many block-support RQD as
374 directions of interest, with no need for the data to be measured along the same direction
375 because RQD can be simulated for each geographical coordinate and each direction (Fig. 9,
376 top left). The regionalization in a 5D space (left panel) therefore allows calculating a
377 directional RQD. All the calculations can be made on each simulation separately or averaged
378 over the 500 simulations to obtain a prediction.
379
380 If a block has to be characterized by a single RQD value, the minimum RQD over all
381 the directions should be considered, which leads to a 'non-directional' block-support RQD
382 (Fig. 9, middle left). In such a case, the change of support is essentially non-additive as it
383 relies on a minimum and not an average over the directions. Since the use of a single RQD
384 value to represent the degree of jointing or fracturing in a block is less informative than a
385 direction-dependent RQD (given the high variability in the angular space), we propose to
386 complement the non-directional (minimum) RQD with an anisotropy index (AI) of jointing
387 degree for rock masses, following Zhen et al. (2018). The AI measures the spread or
388 dispersion of the RQD for each block within the angular space. In this work, the AI of the
389 jointing degree is defined for each block and each simulation as one hundred times the

difference between the maximum and minimum RQD values across all the directions, divided by the maximum RQD value (Fig. 9, bottom left):

$$AI = 100\left(\frac{RQD_{max} - RQD_{min}}{RQD_{max}}\right).$$

Figure 10 shows that the anisotropy index is between 30% to 80%, with a marked contrast in the eastern part of the map close to the sampled area. This anisotropy of the jointing degree for the rock mass (directional variability of RQD) is not negligible and cannot be detected when RQD is regionalized in the three-dimensional geographical space and the directional component is discarded (i.e., using the traditional approach).

In addition to the minimal RQD over all the directions (as the representative value of a block) and the anisotropy index (indicating how much RQD varies from one direction to another), one can identify the direction for which the minimal RQD is reached. This direction sheds light on the anisotropy of the discontinuity network in the rock mass and on the existence of preferential fracturing directions, as in the Terzaghi concept (Zhen et al., 2018) (the minimum RQD is expected to occur along the direction perpendicular to the fracture planes). Such an analysis can be made locally (for a single block) or for a group of blocks. As an illustration, Fig. 11 is an azimuthal projection of the upper hemisphere of an equal-angle polar net (Priest, 1985) showing the directional concentration for the minimum simulated RQD at a regular grid of the geographical space (1,750 blocks) and 100 directions spanning the space at intervals of 36° and 18° in azimuth and dip, respectively, where the gray dots represent the sampling directions. On average, the RQD rating decreases by 20.66% when considering the direction of the minimum value per block due to its directional dependence. The minimum RQD is more frequently reached along directions of azimuth between 330° to 350° and dip between 30° and 45°, or directions with azimuth between 285° and 315° and

416 dip between 30° and 45°. The latter suggests that the fracture planes tend to be sub-
417 horizontal to oblique with a northwest-north direction, similar to the orientation of the parallel
418 structural domain (NW-SE).
419
420 RQD can be predicted at the block support by averaging the simulated RQD over
421 many scenarios, as shown in Figs. 7 and 8 for the composite support. When the results of
422 the 3D traditional approach (Fig. 12a) are compared with those using the directional
423 approach (Fig. 12b-f), several differences arise, highlighting the influence of the directional
424 dependence of RQD in the geomechanical zoning of the rock mass. In essence, Fig. 12a
425 bears more resemblance to Fig. 12e, where RQD is simulated along the north direction, than
426 to Fig. 12e and 12f corresponding to RQD simulated along the east and vertical directions.
427 This reveals a bias of the RQD predicted with the traditional approach, conditioned to
428 particular sampling directions, and cannot be extrapolated to other directions. In contrast, the
429 directional block-support RQD (Fig. 12d-f) is more informative and helpful for geotechnical
430 designs and rock mass rating or geotechnical zoning. Since it is an unbiased representation
431 for a specific direction, it can evaluate the impact of the advance of the rock excavation in
432 this direction in rock mass mechanical behavior.
433
434 To exemplify the impact of directional RQD modeling in engineering decision-making,
435 consider a tunnel bored along the north-south direction with a width of 30 ft (9.4 m) in an
436 igneous/metamorphic rock, typical in the study area, where real rock pressures or
437 swelling/squeezing ground do not exist. According to the rock support classification system
438 based on RQD for tunnels of varying widths (Deere, 1989), either steel sets or reinforced
439 shotcrete or RIB is compulsory almost everywhere if one relies on the RQD corresponding to
440 the worst-case scenario for each block (Fig 12c), which may be too pessimistic. In contrast,
441 based on the directional block-support RQD associated with the tunnel direction (north-
442 south) (Fig 12d), only a pattern bolting (4-6 ft centers) or a 4-6 cm shotcrete is required in the

443 eastern side of the area under study. On the other hand, considering the RQD models
444 obtained with the traditional approach (Fig. 12a) or with the average scenario (Fig 12b)
445 (average RQD over all the directions and all the simulations) gives a misleading
446 representation of the actual rock quality in the eastern part, with a minimal requirement (no
447 support or local bolts, which is too optimistic).

448 *4.5. Geotechnical zoning*

449

450 The lithological characteristics and the degree of alteration are homogeneous in the
451 studied area; therefore, the rock mass quality is the most relevant criterion for its
452 geotechnical zoning. Our results on the upscaled RQD may conveniently be integrated into
453 widely used rock mass classification systems, such as the RMR and its modifications
454 (Bieniawski, 1973, 1989; Hoek et al., 2013; Bertuzzi et al. 2016), the Tunneling Quality Index
455 (Q; Barton et al., 1974) and the Geological Strenght Index (GSI; Marinos and Carter, 2018).
456 Following Deere et al. (1967), we relate our simulated block-averaged RQD value with the
457 engineering rock mass quality and implement a geotechnical zoning map (Fig. 13). For each
458 block and each simulation, the simulated block-support RQD is assigned one of five classes
459 (excellent, good, fair, poor, very poor), then the class that most frequently appears across the
460 500 simulations is retained as the final classification of the block.

461

462 The zoning maps so obtained strongly differ, depending on whether one considers
463 the non-directional RQD calculated with the traditional approach (Fig. 13a), or the average
464 (Fig. 13b) or the minimum (Fig. 13c) RQD over all the directions calculated with the proposed
465 approach. The former approach ignores the directional dependence of RQD and mixes
466 measurements made in different drilling directions. Therefore, the map in Fig. 13a lacks
467 physical sense, where the primary class is a fair quality rock, with 85% of the blocks,
468 followed by a good quality rock with 8%. The remaining are between poor (3.7%) and

469 excellent (3.3%). A similar mixing arises with the map in Fig. 13b: although RQD is
470 regionalized in a 5D space, the simulated values are then averaged over all the directions,
471 yielding zoning similar to the traditional approach (poor 0.3%, fair 88.1%, good 11.5%, and
472 excellent 0.1%). In contrast, the map in Fig. 13c only considers the 'worst' direction for each
473 block (the one associated with the lowest RQD) and yields a more conservative definition of
474 the geotechnical domains, where almost three-quarters of the blocks are classified as poor to
475 fair rock (73.4%) and the rest as very poor. This is the price to pay to get geotechnical zoning
476 that is non-directional and, at the same time, physically meaningful.

477 ## 5. Discussion

478

479 *Contribution of our work*. Like all types of one-dimensional measurements (borehole
480 cores and scanlines), RQD depends not only on the geographical position of the sample but
481 also on its direction, precluding a direct averaging that mixes different directions as a proper
482 upscaling strategy. Upscaling must appropriately address the directional dependence to
483 reduce uncertainties in geotechnical projects. Our proposal considers regionalizing the RQD
484 data in a five-dimensional space corresponding to the three-dimensional geographical space
485 crossed with the two-dimensional sphere, allowing RQD to be interpolated at any place in the
486 geographical space and for any direction. Knowing the rock mass quality in specific
487 directions is beneficial to evaluate the impact of the discontinuity orientations for tunnels,
488 slopes, or foundation designs. The latter becomes critical, bearing in mind that the rock mass
489 behavior is influenced by the regional geological structures rather than by the strength of
490 intact rock, as shown, for instance, by the coincidence of the orientation of minimum RQD
491 values (Fig. 11) with regional structural faults.

492

493 *Applicability*. The 5D geostatistical approach requires sampling data with information
494 on RQD and on the borehole positions and orientations, information that should always be

logged and readily available in any good geotechnical database. The spatial and directional behaviors of RQD can be modeled in a flexible manner, using basic nested structures to fit the experimental variogram of the RQD data. This makes the proposal applicable to an extensive range of rock masses and conditions, including both weak and complex situations, such as tectonized (disturbed and broken by structural dislocation, shearing, folding, or compression) or heterogeneous (flysch formations or molassic formations) rock masses.

Practical limitations. If all the boreholes have the same or almost the same orientation (e.g., vertical), then it can be challenging to infer the directional behavior of RQD and to apply the 5D geostatistics approach. Other practical limitations of this approach are the assumptions of stationarity in the geographical space and isotropy on the sphere (see Appendix). The former assumption is often sensible after partitioning the deposit into areas ('geotechnical domains') with similar structural and mechanical characteristics, and performing the geostatistical analysis within each domain separately. As for the latter assumption of isotropy, it may be questionable when there is only one network of parallel fractures, in which case it would make sense to work with anisotropic variogram models on the sphere.

3D vs. 5D modeling. The traditional (three-dimensional, non-directional) and proposed (five-dimensional, directional) approaches to modeling RQD in rock engineering applications have been cross-validated, providing a good fit in terms of prediction and uncertainty assessment. Each approach has its pros and cons. For lower computational requirements and pre-processing time, the traditional approach achieves a globally good prediction of RQD but is locally biased as per the drilling direction. The directional approach is more demanding in terms of modeling and computational capacity but provides information on the directional RQD behavior, which is valuable for geotechnical zoning and decision-making as it reflects the inherent nature of the geotechnical parameters (their directional

522 dependence) and can give an insight into the geometry of the rock fragments when
523 combined with other direction-dependent parameters such as the fracture frequency. This
524 approach accounts for the fact that, in the presented case study, one measurement of RQD
525 provides much information about values at surrounding locations along the same or nearly
526 parallel directions, as indicated by low variogram values at short separation distances and
527 small separation angles (Fig. 5). However, an RQD measurement provides less information
528 in a perpendicular direction. Therefore, it constitutes good practice to account for the
529 directional dependence of RQD in any geostatistical modeling and upscaling analysis.

530 ## 6. Conclusions and perspectives

531

532 The common practice in geotechnical modeling overlooks the directional dependence
533 of geotechnical variables and characterizes volumetric support assuming rock masses as a
534 continuum and isotropic medium and extrapolating or averaging sample-support information
535 (from boreholes or scanlines) to a three-dimensional block support or to the rock mass.
536 However, rock masses are seldom isotropic and are generally heterogeneous, hence our
537 proposal to tackle the change of support problem by accounting for the inherent directional
538 dependence of RQD (5D regionalization) and for its uncertainty at unsampled locations (use
539 of geostatistical simulations). This change of support is performed by averaging the RQD
540 simulated along a specific direction on a grid, discretizing each block in the geographical
541 space. The upscaled directional RQD is practical, simple, and does not modify the original
542 concept of RQD, making it suitable and serviceable in engineering applications, e.g., to
543 determine required tunnel support. The directional approach better reproduces the
544 geographical and directional heterogeneity and real nature of the rock mass. A non-
545 directional upscaled RQD can also be derived from this approach by considering the
546 minimum value obtained over all the directions (corresponding to the most unfavorable
547 direction of fracturing, i.e., the worst case scenario) and complemented with an anisotropy

548 index of jointing degree (sensu Zheng et al., 2018). Both the directional and non-directional
549 RQD so obtained directly impact the prediction of safety factors and control measures in rock
550 engineering projects.
551
552 Our directional approach can be used for geotechnical zoning (Fig. 13), i.e.,
553 classifying the rock mass into similar design areas. Besides helping determine fault zones,
554 and by applying empirical formulas, it is also possible to calculate other mechanical
555 parameters such as the modulus of elasticity or the unconfined compressive strength (Zhang
556 and Einstein, 2004, Zhang, 2016). This approach is helpful in any stage of a geotechnical
557 project. At the exploratory or early stages, it is suggested to use adaptive geometries in the
558 block model: the size of the block will depend on the variability of the geotechnical parameter
559 in the sector and the available information, i.e., the less amount of available information (and
560 the more variability of RQD), the larger the block size. At the development and production
561 stages, it is possible to model the geotechnical parameters, whether in a parallel or
562 perpendicular direction, to advance the construction of the excavation in rock.
563
564 One way to optimize the analysis is to use adaptive geometries in the block model in
565 further developments, giving a higher resolution (smaller block size) in areas with a higher
566 anisotropy index or vice versa. Moreover, for upscaling directional variables such as RQD, it
567 is interesting to analyze the relationship between strength and stiffness versus block size to
568 determine the Representative Volume Element size, REV (Zhang et al., 2017).
569
570 To broaden the scope of application of the presented proposal, future works in the 5D
571 geostatistical modeling should include the design of variogram models and simulation
572 algorithms using non-separable covariance functions or anisotropic covariances on the
573 sphere, together with exploratory tools to identify preferred directions of anisotropy on the
574 sphere based on sampling information.

Acknowledgments

The authors acknowledge the funding of the National Agency for Research and Development of Chile, through postgraduate study scholarship ANID-PFCHA/Doctorado Nacional/2019-21190855 and grants ANID PIA AFB180004 and ANID / FONDECYT / REGULAR / N°1170101, and of the CSIRO-Chile International Center of Excellence in Mining and Mineral Processing. The main author is also grateful to ARMINES and Mines ParisTech for logistical support and to H. Rivera for providing many constructive comments that helped to improve the manuscript. We are also indebted to an anonymous reviewer and the editor Janusz Wasowski for their constructive and thoughtful reviews.

References

Azimian, A., 2016. A new method for improving the RQD determination of rock core in borehole. Rock Mechanics and Rock Engineering, 49(4), 1559-1566.

Bandis, S., Lumsden, A.C., Barton, N.R., 1981. Experimental studies of scale effects on the shear behaviour of rock joints. International Journal of Rock Mechanics and Mining Sciences & Geomechanics Abstracts, 18(1), 1–21.

Barton, N., 1990. Scale effects or sampling bias? In Proceedings of the 1st International Workshop Scale Effects in Rock Masses, Loen, Norway, 7–8 June 1990; Balkema: Rotterdam, The Netherlands; pp. 31–55.

Barton, N., Reidar, L., Lunde, J., 1974. Engineering classification of rock masses for the design of tunnel support. Rock mechanics 6(4), 189–236.

Bertuzzi, R., Douglas, K., Mostyn, G., 2016. Comparison of quantified and chart GSI for four rock masses. Engineering Geology, 202, 24–35.

Bieniawski, Z.T., 1968. The effect of specimen size on compressive strength of coal. International Journal of Rock Mechanics and Mining Sciences & Geomechanics Abstracts, 5(4), 325–326.

Bieniawski, Z.T., 1973. Engineering classification of jointed rock masses. Civil Engineer in South Africa, 15(12), 343–353.

Bieniawski, Z.T., 1989. Engineering Rock Mass Classifications: a Complete Manual for Engineers and Geologists in Mining, Civil, and Petroleum Engineering. John Wiley & Sons, New York.

Boyd, D.L., Walton, G., Trainor-Guitton, W., 2019. Quantifying spatial uncertainty in rock through geostatistical integration of borehole data and a geologist's cross-section. Engineering Geology, 260, 105246.

Cai, M., 2011. Rock mass characterization and rock property variability considerations for tunnel and cavern design. Rock mechanics and rock engineering, 44(4), 379-399.

Chen, J.Q., Li, X.J., Zhu, H.H., Rubin, Y., 2017. Geostatistical method for inferring RMR ahead of tunnel face excavation using dynamically exposed geological information. Engineering Geology, 228, 214-223.

Chilès, J.P., Delfiner, P., 2012. Geostatistics: Modeling Spatial Uncertainty. Wiley, New York, 699 pp.

Choi, S.Y., Park, H.D., 2004. Variation of rock quality designation (RQD) with scanline orientation and length: a case study in Korea. International Journal of Rock Mechanics and Mining Sciences, 41(2), 207-221.

Choi, Y., Yoon, S.Y., Park, H.D., 2009. Tunneling Analyst: a 3D GIS extension for rock mass classification and fault zone analysis in tunneling. Computers & Geosciences 35(6): 1322–1333.

Chowdhury, R., Flentje, P., Bhattacharya, G., 2012. Geotechnics in the 21st century, uncertainties and other challenges, with particular references to landslide hazard and risk assessment. J. Life Cycle Reliab. Saf. Eng., 1, 27–43.

625 Cuisiat, F.D., Haimson, B.C., 1992. Scale effects in rock mass stress measurements.
626 International Journal of Rock Mechanics and Mining Sciences & Geomechanics Abstracts,
627 29(2), 99-117.
628 Cunha, A.P., 1990. Scale effects in rock mechanics. In: Proocedings of the first
629 International workshop on scale effect in rock masses, Loen, 7-8 June, 3-31.
630 Deere, D.U., 1989. Rock quality designation (RQD) after 20 years. US Army Corps
631 Engrs. Contract Report GL-89-1. Waterways Experimental Station, Vicksburg, MS.
632 Deere, D.U., Hendron Jr, A.J., Patton, F.D., Cording, E.J., 1967. Design of surface
633 and near-surface construction in rock. In: Failure and Breakage of Rock, Proceedings of the
634 Eighth Symposium on Rock Mechanics, American Institute of Mining and Metallurgical
635 Engineers (pp. 273-303).
636 Edelbro, C., 2004. Evaluation of rock mass strength criteria. Doctoral dissertation,
637 Luleå Tekniska Universitet.
638 Elsayed, A.E., Sen, Z., 1991. Probabilistic simulation of rock quality designation
639 (RQD). Bulletin of the International Association of Engineering Geology-Bulletin de
640 l'Association Internationale de Géologie de l'Ingénieur, 43(1), 31-40.
641 Emery, X., Lantuéjoul, C., 2006. TBSIM: A computer program for conditional
642 simulation of three-dimensional Gaussian random fields via the turning bands method.
643 Computers & Geosciences, 32(10), 1615–1628.
644 Emery, X., Porcu, E., 2019. Simulating isotropic vector-valued Gaussian random
645 fields on the sphere through finite harmonics approximations. Stochastic Environmental
646 Research and Risk Assessment, 33(8-9), 1659–1667.
647 Emery, X., Séguret, S.A., 2020. Geostatistics for the Mining Industry - Applications to
648 Porphyry Copper Deposits. CRC Press, Boca Raton, 247 pp.
649 Exadaktylos, G., Stavropoulou, M., 2008. A specific upscaling theory of rock mass
650 parameters exhibiting spatial variability: Analytical relations and computational scheme.
651 International Journal of Rock Mechanics and Mining Sciences, 45(7), 1102–1125.

652 Ferrari, F., Apuani, T., Giani, G.P., 2014. Rock Mass Rating spatial estimation by
653 geostatistical analysis. International Journal of Rock Mechanics and Mining Sciences, 70,
654 162–176.
655 Gao, X., Yan, E.C., Yeh, T.C.J., Cai, J.S., Liang, Y., Wang, M., 2018. A geostatistical
656 inverse approach to characterize the spatial distribution of deformability and shear strength
657 of rock mass around an unlined rock cavern. Engineering Geology, 245, 106–119.
658 Goovaerts, P., 2001. Geostatistical modelling of uncertainty in soil science.
659 Geoderma 103: 3–26.
660 Haftani, M., Chehreh, H.A., Mehinrad, A., Binazadeh, K., 2016. Practical
661 investigations on use of weighted joint density to decrease the limitations of RQD
662 measurements. Rock Mechanics and Rock Engineering, 49(4), 1551-1558.
663 Hekmatnejad, A., Emery, X., Brzovic, A., Schachter, P., Vallejos, J.A., 2017. Spatial
664 modeling of discontinuity intensity from borehole observations at El Teniente mine, Chile.
665 Engineering Geology 228: 97-106.
666 Hoek, E., 2006. Practical Rock Engineering. Rocscience: Rock mass classification
667 Hoek, E., Brown, E.T., 1980. Underground Excavations in Rock. Inst. Min. Metall.
668 London: Stephen Austin and Sons, 527.
669 Hoek, E., Carter, T.G., Diederichs, M.S., 2013. Quantification of the geological
670 strength index chart. In 47th US rock mechanics/geomechanics symposium. American Rock
671 Mechanics Association.
672 Hudson, J., 2012. Design methodology for the safety of underground rock
673 engineering. Journal Rock Mechanics and Geotechnical Engineering, 4, 205–214.
674 Journel, A.G., 1983. Non-parametric estimation of spatial distributions. Mathematical
675 Geology, 15(3), 445–468.
676 Lantuéjoul, C., Freulon, X., Renard, D., 2019. Spectral simulation of isotropic
677 Gaussian random fields on a sphere. Mathematical Geosciences, 51(8), 999-1020.

678 Madani, N., Asghari, O., 2013. Fault detection in 3D by sequential Gaussian
679 simulation of Rock Quality Designation (RQD). Arabian Journal of Geosciences 12(10):
680 3737-3747.
681 Marinos, V.I.I.I., Marinos, P., Hoek, E., 2005. The geological strength index:
682 applications and limitations. Bulletin of Engineering Geology and the Environment, 64(1), 55-
683 65.
684 Marinos, V., Carter, T.G., 2018. Maintaining geological reality in application of GSI for
685 design of engineering structures in rock. Engineering Geology, 239, 282-297.
686 Matheron, G., 1973. The intrinsic random functions and their applications. Advances
687 in Applied Probability, 5(3), 439-468.
688 Matonti, C., Guglielmi, Y., Viseur, S., Bruna, P. O., Borgomano, J., Dahl, C., Marié, L.,
689 2015. Heterogeneities and diagenetic control on the spatial distribution of carbonate rocks
690 acoustic properties at the outcrop scale. Tectonophysics, 638, 94-111.
691 Oh, S., Chung, H., Kee Lee, D., 2004. Geostatistical integration of MT and boreholes
692 data for RMR evaluation. Environmental Geology, 46, 1070–1078.
693 Ozturk, C.A., Nasuf, E., 2002. Geostatistical assessment of rock zones for tunneling.
694 Tunnelling and Underground Space Technology, 17, 275–285.
695 Ozturk, C.A., Simdi, E., 2014. Geostatistical investigation of geotechnical and
696 constructional properties in Kadikoy–Kartal subway, Turkey. Tunnelling and Underground
697 Space Technology, 4, 35–45.
698 Palmström, A., 1982 The volumetric joint counted useful and simple measure of the
699 degree of rock mass jointing. In: Proceedings of the 4th Congress of International
700 Association of Engineering Geology, pp. 221e8. New Delhi.
701 Palmström, A., 2005. Measurements of and correlations between block size and rock
702 quality designation (RQD). Tunnelling and Underground Space Technology, 20(4), 362-377.

Pinheiro, M., Vallejos, J., Miranda, T., Emery, X., 2016. Geostatistical simulation to map the spatial heterogeneity of geomechanical parameters: a case study with rock mass rating. Engineering Geology, 205, 93-103.

Pratt, H.R., Black, A.D., Brown, W.S., Brace, W.F., 1972. The effect of speciment size on the mechanical properties of unjointed diorite. International Journal of Rock Mechanics and Mining Sciences & Geomechanics Abstracts, 9(4), 513-516.

Priest, S.D., 1985. Hemispherical projection methods in rock mechanics. Allen & Unwin.

Priest, S.D., Hudson, J.A., 1976. Discontinuity spacings in rock. International Journal of Rock Mechanics and Mining Sciences & Geomechanics Abstracts, 13(5), 135-148.

Pinheiro, M., Vallejos, J.A., Miranda, T., Emery, X., 2016. Geostatistical simulation to map the spatial heterogeneity of geomechanical parameters: A case study with rock mass rating. Engineering Geology, 205, 93-103.

Sánchez, L.K., Emery, X., Séguret, S.A., 2019. 5D geostatistics for directional variables: Application in geotechnics to the simulation of the linear discontinuity frequency. Computers & Geosciences, 133, 104325.

Schoenberg, I.J., 1942. Positive definite functions on spheres. Duke Mathematics Journal, 9(1), 96–108.

Séguret, S.A., Guajardo, C., 2015. Geostatistical evaluation of rock quality designation & its link with linear fracture. In: Schaeben, H., Tolosana Delgado, R., van den Boogaart, K.G., van den Boogaart, R. (eds.), Proceedings of IAMG 2015 - 17th Annual Conference of the International Association for Mathematical Geosciences. Curran Associates, Red Hook, NY, pp. 1043–1051.

Séguret, S.A., Guajardo, C., Freire, R., 2014. Geostatistical evaluation of fracture frequency and crushing. In: Castro, R. (ed.), Proceedings of the 3rd International Symposium on Block and Sublevel Caving. Universidad de Chile, Santiago, pp. 280–288.

729 Sen, Z., Kazi, A., 1984. Discontinuity spacing and RQD estimates from finite length
730 scanlines. International Journal of Rock Mechanics and Mining Sciences & Geomechanics
731 Abstracts, 21(4), 203-212.
732 Song, K.I., Cho, G.C., Lee, S.W., 2011. Effects of spatially variable weathered rock
733 properties on tunnel behavior. Probabilistic Engineering Mechanics, 26(3), 413-426.
734 Stavropoulou, M., Exadaktylos, G., Saratsis, G., 2007. A combined three-dimensional
735 geological/geostatistical numerical model of underground excavations in rock. Rock
736 Mechanics and Rock Engineering, 40(3), 213-243.
737 Vatcher, J., McKinnon, S.D., Sjöberg, J., 2016. Developing 3-D mine-scale
738 geomechanical models in complex geological environments, as applied to the Kiirunavaara
739 Mine. Engineering Geology, 203, 140-150.
740 Zhang, L., 2016. Determination and applications of rock quality designation (RQD).
741 Journal of Rock Mechanics and Geotechnical Engineering, 8(3), 389-397.
742 Zhang, L., Einstein, H.H., 2004. Using RQD to estimate the deformation modulus of
743 rock masses. International Journal of Rock Mechanics and Mining Sciences (1997), 41(2),
744 337-341.
745 Zhang, L., Xia, L., Yu, Q., 2017. Determining the REV for fracture rock mass based
746 on seepage theory. Geofluids, 2017.
747 Zheng, J., Yang, X., Lü, Q., Zhao, Y., Deng, J., Ding, Z., 2018. A new perspective for
748 the directivity of Rock Quality Designation (RQD) and an anisotropy index of jointing degree
749 for rock masses. Engineering Geology, 240, 81-94.

750 ## Appendix A

751 *A.1. Traditional approach: modeling RQD in the 3D Euclidean space*

752

753 This approach considers that RQD varies only with the geographical coordinates
754 (easting, northing, and elevation), i.e., regionalized in the Euclidean space $\mathbb{R}^3$. A common
755 practice for geostatistical modeling is to assume second-order stationarity, i.e., the mean
756 value and the covariance function or the variogram are invariant under a translation in space,
757 which allows their inference from a set of sampling data (Chilès and Delfiner, 2012). A
758 convenient way to model the experimental covariance (or experimental variogram) is through
759 a positive linear combination of basic nested structures:

760 $$C(\boldsymbol{h}) = cov\{Z(\boldsymbol{x}+\boldsymbol{h}), Z(\boldsymbol{x})\} = \sum_{s=1}^{Smax} b_s\, \rho_s(\boldsymbol{h}) \qquad (A.1)$$

761 where Z is the Gaussian random field associated with RQD, ***x*** and ***x***+***h*** are two points in the
762 geographical space separated by vector ***h*** and, for s = 1,… S_{max}, b_s is a nonnegative real
763 value, and ρ_s is an autocorrelation function (positive semi-definite function taking the value 1
764 at ***h*** = **0**).

765 The Gaussian random field can then be simulated as a sum of S_{max} components,
766 each associated with a particular nested structure:

767 $$Z^{(S)}(\boldsymbol{x}) = \sum_{s=1}^{Smax} \sqrt{b_s}\, Z_s^{(S)}(\boldsymbol{x}) \qquad (A.2)$$

768 where the superscript (S) stands for 'simulated'. The reader is referred to Emery and
769 Lantuéjoul (2006) for algorithmic details on the simulation process for the nested structures
770 commonly used in geostatistical applications.

771 *A.2. Directional approach: modeling in a 5D product space*

772

773 To account for the fact that RQD is direction-dependent, the associated random field
774 Z is now defined in a five-dimensional space ($\mathbb{R}^3 \times \mathbb{S}^2$, with $\mathbb{S}^2$ the unit sphere), i.e., Z =

{Z(***x***,***u***): ***x*** ∈ $\mathbb{R}^3$ and ***u*** ∈ $\mathbb{S}^2$}, where ***x*** represents the geographical coordinates of the measurement, and ***u*** the direction (azimuth and dip) of this measurement.

The simplest way to model the spatial correlation of regionalized data in such a 5D space is to consider second-order stationarity in the geographical space and second-order isotropy on the sphere. These assumptions imply that the mean value is constant and that the covariance function or the variogram between the two random variables located at (***x***,***u***) and (***x′***,***u′***) in $\mathbb{R}^3 \times \mathbb{S}^2$ only depends on the separation vector ***h*** = ***x′***-***x*** and on the geodesic distance or angular separation $\delta(\boldsymbol{u},\boldsymbol{u}') = \arccos(\langle \boldsymbol{u},\boldsymbol{u}' \rangle)$, with < , > the inner product. The modeling can be extended as follows:

$$C(\boldsymbol{h},\delta) = \sum_{s=1}^{S_{max}} b_s C_s(\boldsymbol{h},\delta) \qquad (A.3)$$

where, $b_s \geq 0$ for $s = 1,\ldots S_{max}$ and C_s is a basic autocorrelation (positive semi-definite) function defined on $\mathbb{R}^3 \times [0, \pi]$. In this work, separable basic autocorrelation functions are used:

$$C_s(\boldsymbol{h},\delta) = \rho_s(\boldsymbol{h}) P_{n(s)}(\cos\delta) \qquad (A.4)$$

where ρ_s is an autocorrelation function in $\mathbb{R}^3$ and P_n the Legendre polynomial of degree n. Schoenberg (1942) showed that the mapping $\delta \mapsto P_n(\cos\delta)$ is an isotropic correlation function on the sphere. Because the Legendre polynomial P_n has the same parity as n, and because the RQD measurement along a direction ***u*** is the same as along the opposite direction -***u***, the covariance should remain the same when changing $\delta(\boldsymbol{u},\boldsymbol{u}')$ into π-$\delta(\boldsymbol{u},\boldsymbol{u}')$,

799 i.e., when changing $P_n(\cos\delta)$ into $P_n(-\cos\delta)$. Accordingly, only even degrees $n(s)$ should be
800 considered in Eq. (A.4).

801 As for the previous approach, the Gaussian random field can be simulated as a sum
802 of S_{max} components. Each component is associated with a particular nested structure and
803 separates into the product of a geographical component and a directional component
804 (Sanchez et al., 2019):

805 $$Z^{(S)}(\boldsymbol{x},\boldsymbol{u}) = \sum_{s=1}^{Smax} \sqrt{b_s}\, Z_s^{(S)}(\boldsymbol{x}) W_s^{(S)}(\boldsymbol{u}) \qquad (A.5)$$

806

807 with $Z_s^{(S)}(\boldsymbol{x})$ a zero-mean random field in the Euclidean space with autocorrelation $\rho_s(\boldsymbol{h})$, and
808 $W_s^{(S)}(\boldsymbol{u})$ a zero-mean random field on the sphere with autocorrelation $P_{n(s)}(\cos\delta)$, see Emery
809 and Porcu (2019) or Lantuéjoul et al. (2019) for examples on how to simulate random fields
810 on the sphere.

Tables

	Horizontal variograms	Vertical variograms
Azimuth (°)	0, 90, 0	0, 0, 0
Dip (°)	0, 0, 45	90, 0, 135
Lag separation (m)	10	10
Number of lags	45	45
Angular separation between data (°)	0, 30, 60, 90	0, 30, 60, 90
Azimuth tolerance (°)	90, 20, 90	90, 20, 90
Dip tolerance (°)	20	20, 90, 20
Lag tolerance (m)	5.0	5.0
Angular separation tolerance (°)	15	15

Table 1. Parameters for experimental variogram calculations

Figure captions

Figure 1. Geographical and angular spaces. Each core sample (blue cylinder) is indexed by the easting, northing and vertical coordinates of its gravity center in the geographical space, as well as its azimuth and dip in the angular space, totaling 5 coordinates. The measured RQD values depend on both the geographical and angular coordinates.

Figure 2. Block modeling of rock mass class (based on rock quality designation observed at 3800 core samples) in a volume of 350 m along the east direction, 500 m along the north direction, and 700 m along the vertical direction (polymetallic deposit). The classes can be associated with lithological and structural characteristics of the deposit.

Figure 3. Experimental histogram of Rock Quality Designation (RQD) of borehole data composited at a length of 3 m.

Figure 4. Experimental variograms of normal scores data in horizontal, vertical, and oblique directions, for geographical separations ranging from 0 to 500 m and angular separations equal to (a) 0°, (b) 30°, (c) 60°, and (d) 90°. The geographical separation measures the distance between the gravity centers of the paired samples, while the angular separation measures the difference between their orientations (e).

Figure 5. Experimental (asterisks) and modeled (solid lines) variograms of the normal scores data for geographical separation distances ranging from 0 to 150 m and angular separations between paired data ranging from 0° to 90°.

Figure 6. Leave-one-out cross-validation results: (a, c) scatter plots between true RQD (vertical axis) at the sampling locations and the average of 500 simulations (horizontal axis) conditioned to the data in a neighborhood of the target location (excluding the five nearest composites on either side of the same borehole), and (b, d) accuracy plots showing the proportion of data belonging to a probability interval as a function of the interval probability, (a, b) for traditional and (c, d) directional approaches.

847 **Figure 7.** Simulation of RQD using the traditional approach (ignoring directional dependence and regionalizing
848 RQD in the 3D geographical space only). (a) Map of the first simulation. (b) Map of the average of 500
849 simulations. Black dots correspond to the borehole data distant less than 10 m from the grid, and the contour
850 represents the envelope of the kriging variance equal to 0.9 times the data variance.
851
852 **Figure 8.** Simulation of RQD using the directional approach (regionalizing RQD in the 3D geographical space
853 crossed with the 2D angular space). (a, c, e) Maps of the first simulation for (a) north, (c) east, and (e) vertical
854 target directions. (b, d, f) Maps of the average by direction of 500 simulations for (b) north, (d) east, and (f) vertical
855 target directions. Black dots correspond to the borehole data distant less than 10 m from the grid and 45° from the
856 target direction. The contour represents the envelope of the kriging variance equal to 0.9 times the data variance.
857
858 **Figure 9.** A synthesis of the different upscaling proposals. Ns stands for the number of samples per block, Nb for
859 the number of blocks in the geographical space, Nk for the number of simulations, and Nj for the number of
860 directions in the angular space.
861
862 **Figure 10.** Map of anisotropy index (AI) of jointing degree using the directional approach (average index over 500
863 simulations). The blue contour represents the envelope inside which the kriging variance in all the directions is
864 less than 0.9 times the data variance (intersection of the directional envelopes as defined in Fig. 8). The black
865 contour represents the envelope inside which the kriging variance in at least one direction is less than 0.9 times
866 the data variance (union of the directional envelopes as defined in Fig. 8). Both envelopes enclose 'confidence
867 regions' in which the borehole data are informative.
868
869 **Figure 11.** Upper hemispherical equal angle polar projection net or regionalized azimuthal projection showing the
870 concentration of the directions for which the minimum block-support RQD is reached. Calculations consider 500
871 simulations and 1,750 blocks of 10 × 10 × 20 m in a horizontal section of the geographical space. The sphere is
872 discretized into 100 directions. Concentric circles represent the dip/plunge each 30°, increasing from outside and
873 azimuths measured clockwise in degrees from north indicated in the out end the projection. The grey dots
874 correspond to the sampling directions of the borehole data.
875
876 **Figure 12.** Map of the average of 500 simulations of block-support RQD obtained with the (a) 3D traditional
877 approach and with the directional approach; (b) average block-support RQD over all the directions; (c) minimum
878 block-support RQD over all the directions; directional block-support RQD along the (d) north, (e) east and (f)

879 vertical directions. The maps in (a) and (b) mix different directions and do not have a clear physical meaning,
880 while the maps in (c-f) only refer to a single direction per block (most conservative direction in (c), which may vary
881 from block to block, and fixed direction in the other maps).
882
883 **Figure 13.** Geotechnical zoning map using block-support (upscaled) RQD. (a) The most probable class is based
884 on 500 simulations obtained with the traditional 3D approach. (b) and (c) Most probable class based on 500
885 simulations obtained with the 5D directional approach: average over all the directions (b) and minimum RQD over
886 all the directions (c).

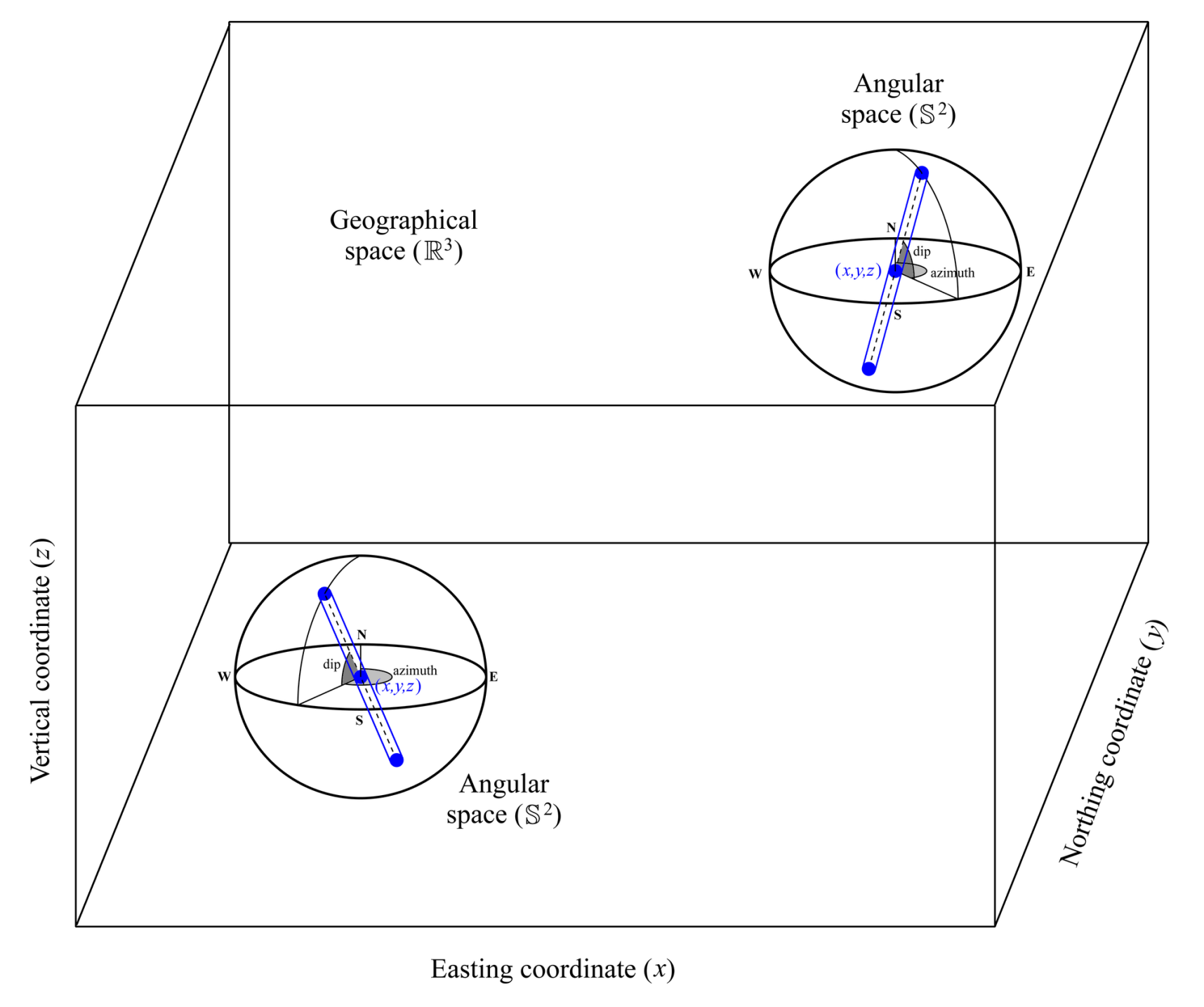
Angular
space ($\mathbb{S}^2$)
Geographical
space ($\mathbb{R}^3$)
N
W
E
S
dip
azimuth
(x,y,z)
Angular
space ($\mathbb{S}^2$)
Vertical coordinate (z)
Northing coordinate (y)
Easting coordinate (x)

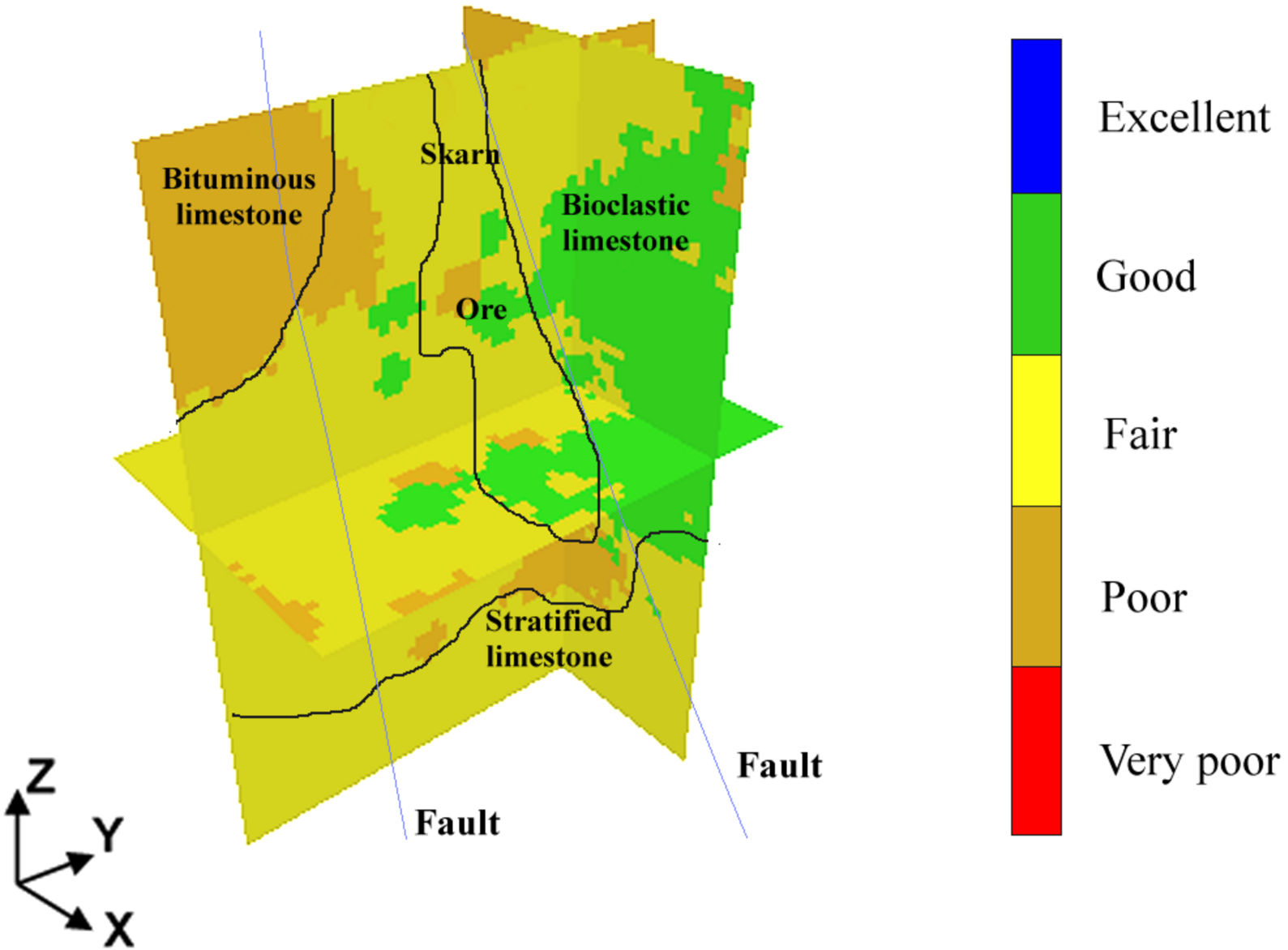
Bituminous limestone
Skarn
Bioclastic limestone
Ore
Stratified limestone
Fault
Fault
Z
Y
X
Excellent
Good
Fair
Poor
Very poor

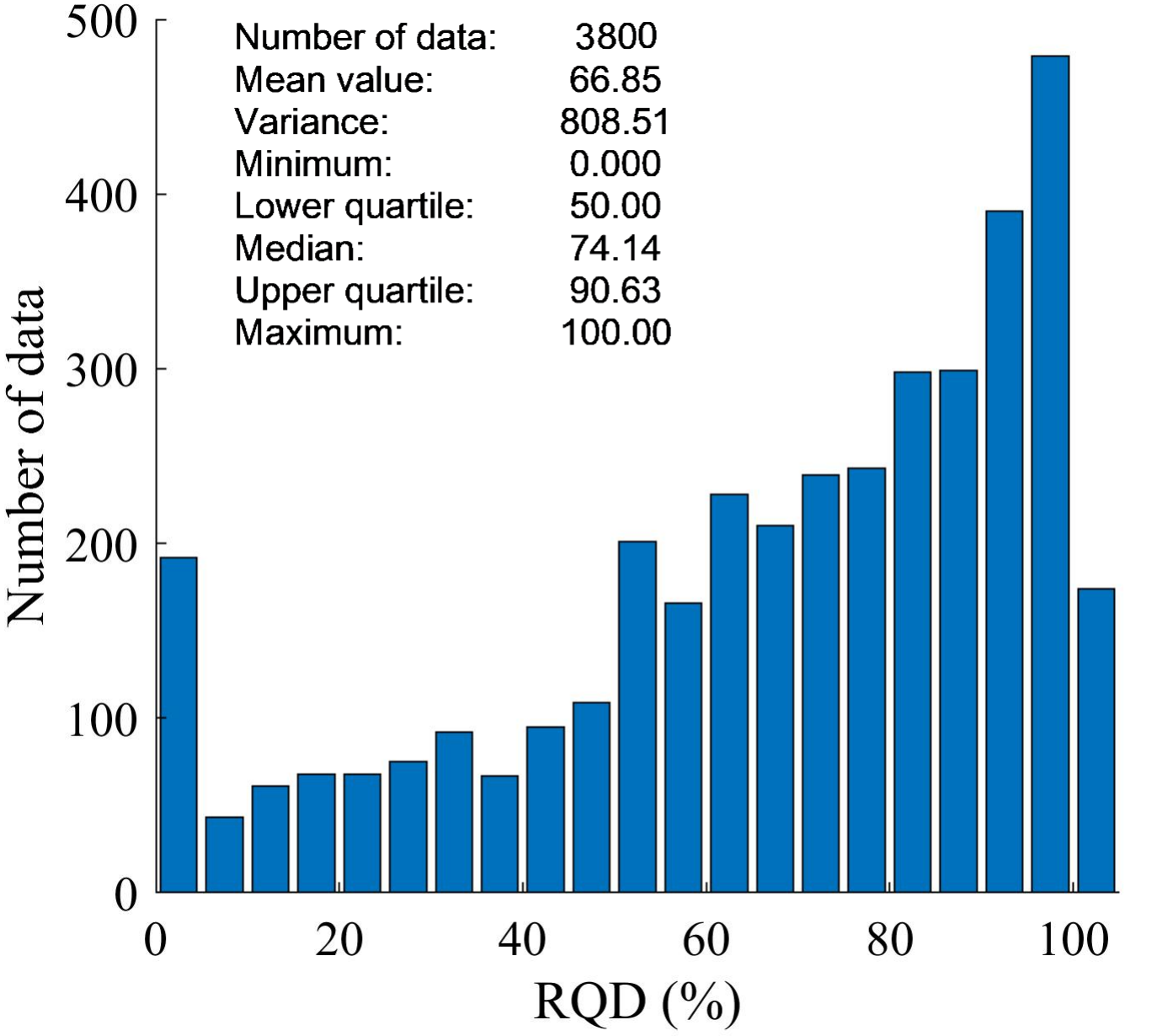
Number of data: 3800
Mean value: 66.85
Variance: 808.51
Minimum: 0.000
Lower quartile: 50.00
Median: 74.14
Upper quartile: 90.63
Maximum: 100.00
500
400
300
200
100
0
Number of data
0
20
40
60
80
100
RQD (%)

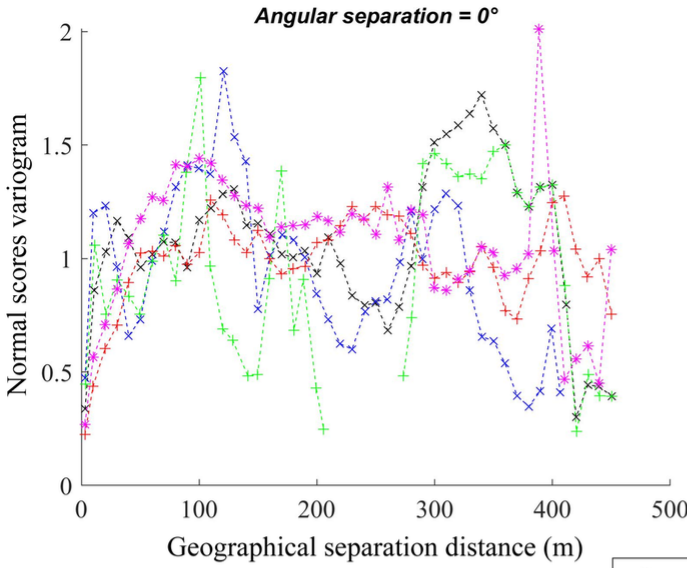
Angular separation = 0°
Normal scores variogram
Geographical separation distance (m)

(a)

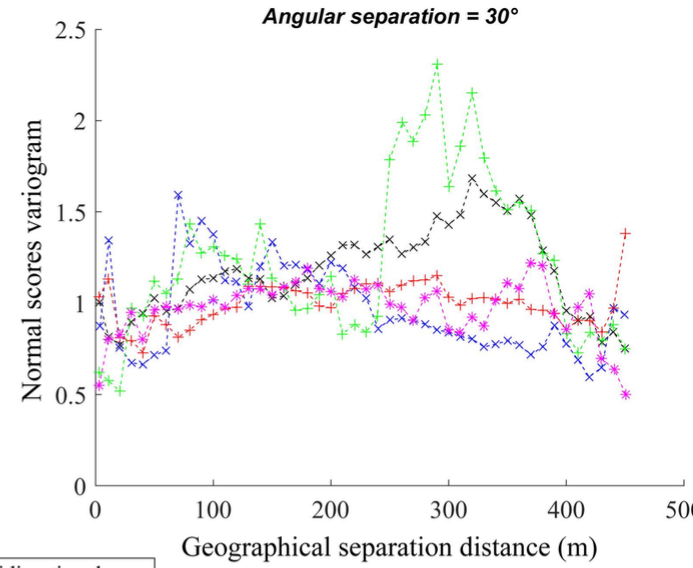
Angular separation = 30°
Normal scores variogram
Geographical separation distance (m)

(b)

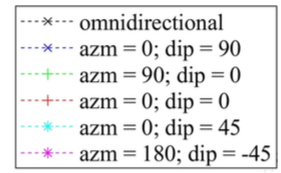
omnidirectional
azm = 0; dip = 90
azm = 90; dip = 0
azm = 0; dip = 0
azm = 0; dip = 45
azm = 180; dip = -45

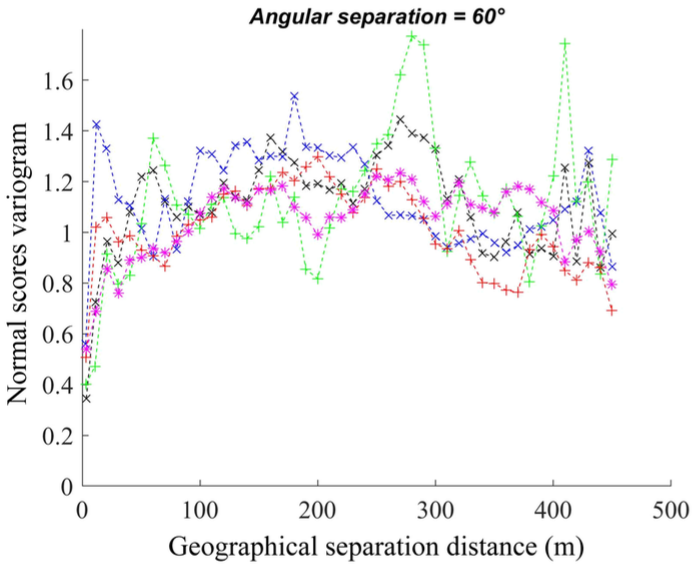
Angular separation = 60°
Normal scores variogram
Geographical separation distance (m)

(c)

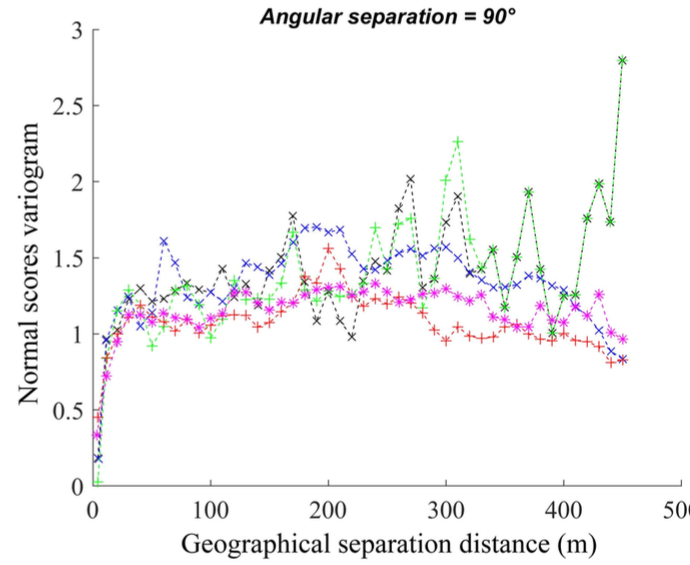
Angular separation = 90°
Normal scores variogram
Geographical separation distance (m)

(d)

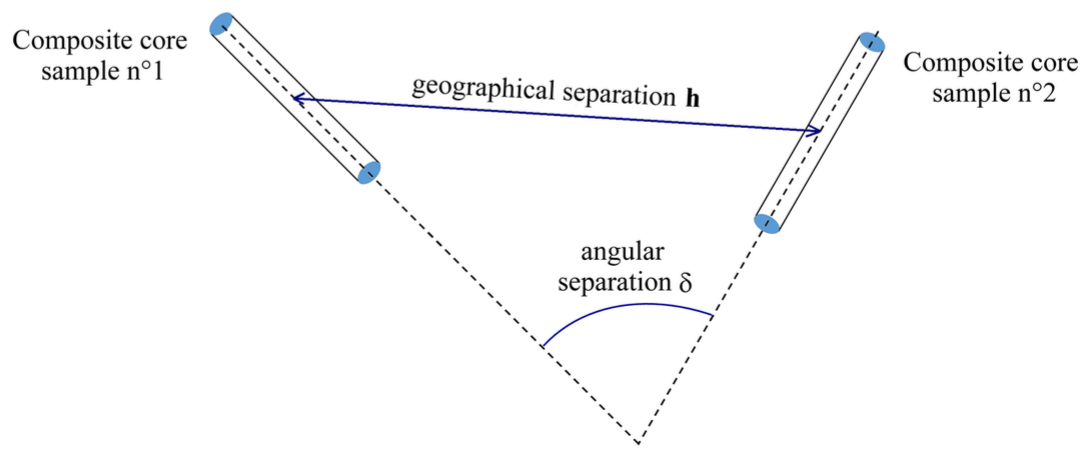
Composite core sample n°1
geographical separation h
Composite core sample n°2
angular separation δ

(e)

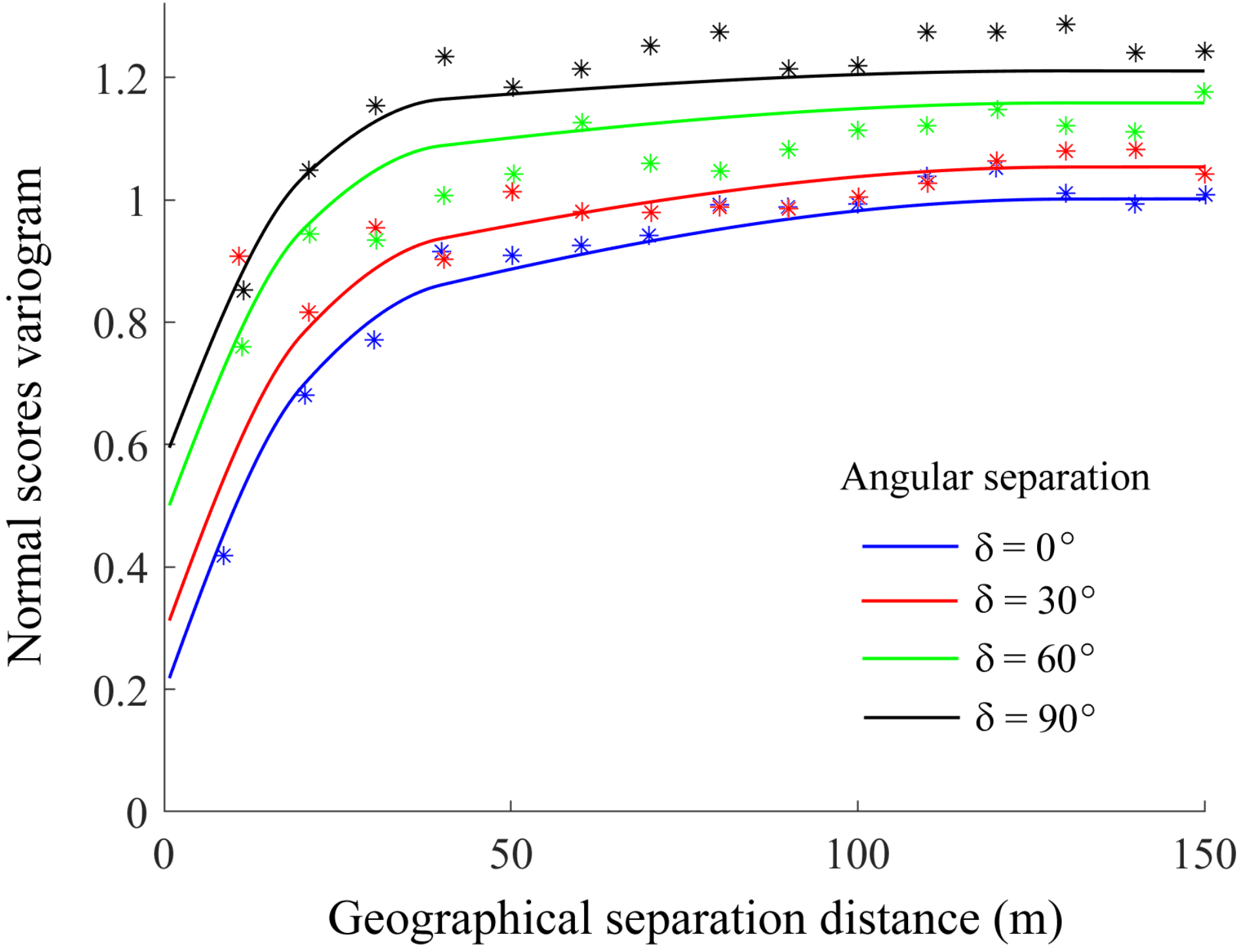
Normal scores variogram
1.2
1
0.8
0.6
0.4
0.2
0
0
50
100
150
Geographical separation distance (m)
Angular separation
δ = 0°
δ = 30°
δ = 60°
δ = 90°

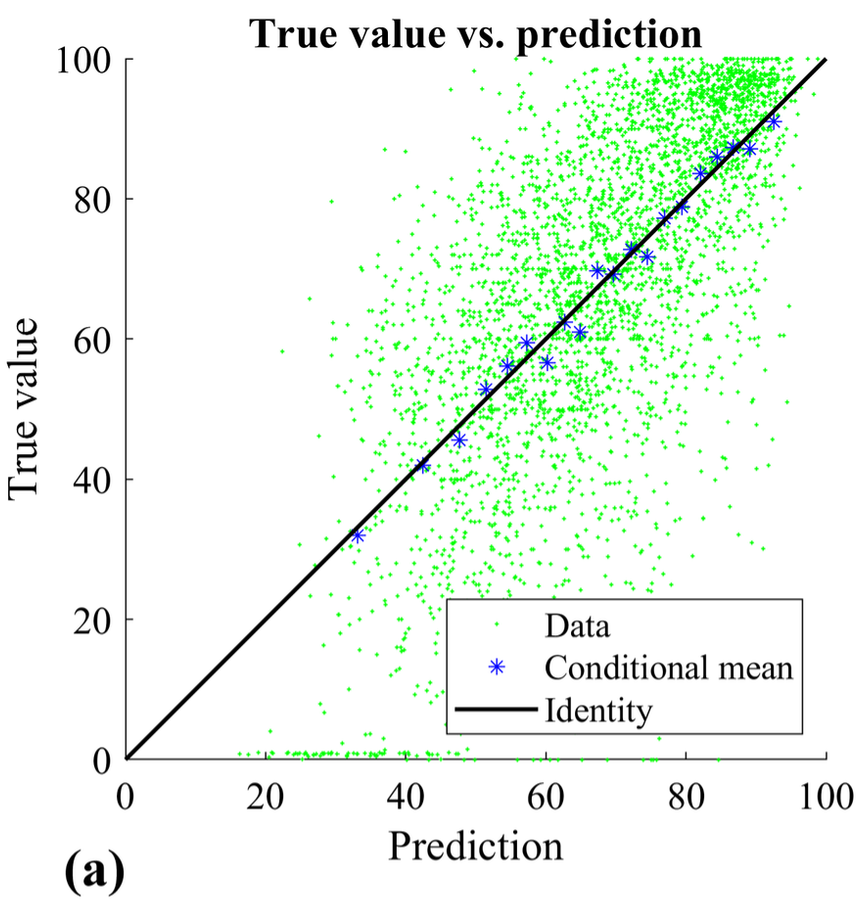
True value vs. prediction
True value
Prediction
Data
Conditional mean
Identity
0
20
40
60
80
100

(a)

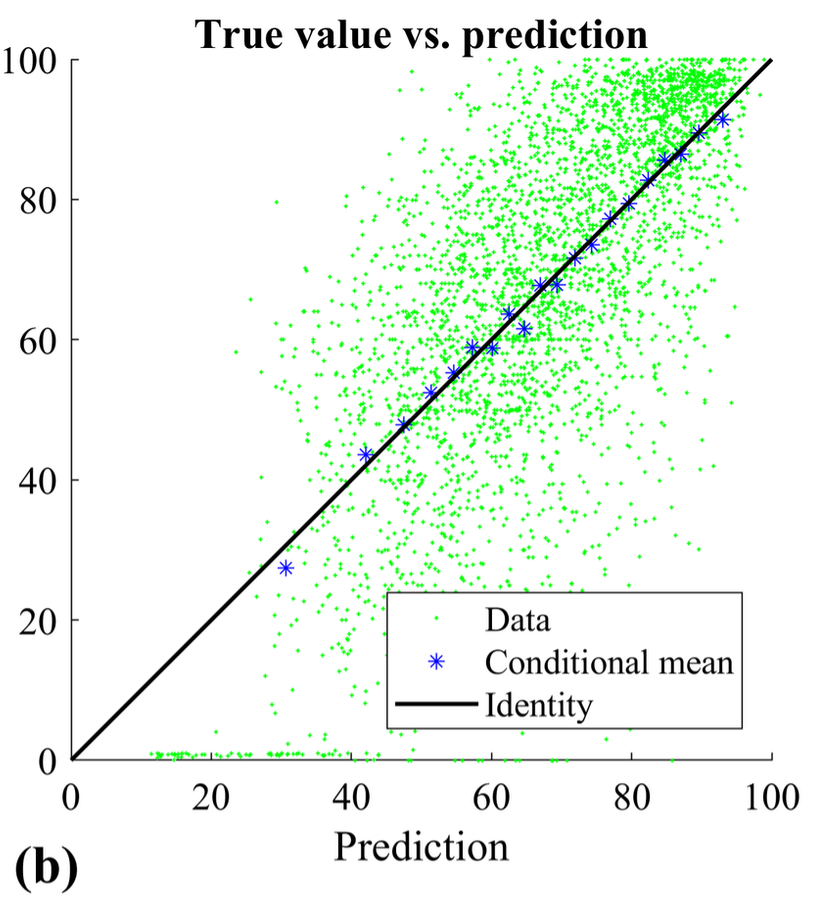
True value vs. prediction
Prediction
Data
Conditional mean
Identity
0
20
40
60
80
100

(b)

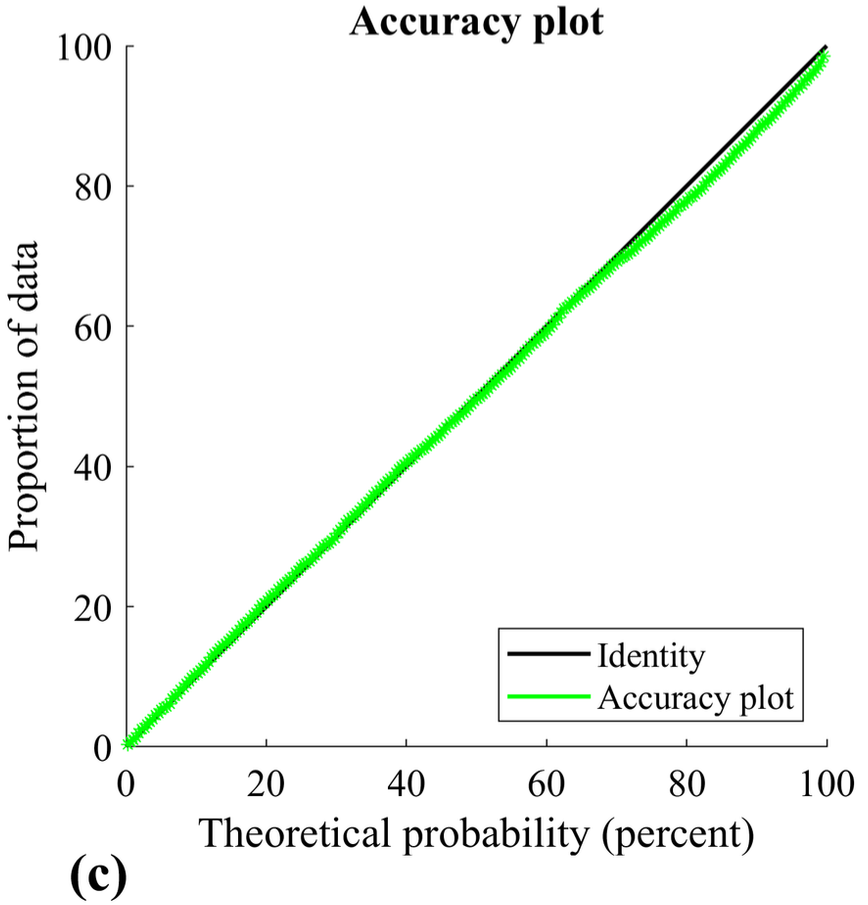
Accuracy plot
Proportion of data
Theoretical probability (percent)
Identity
Accuracy plot
0
20
40
60
80
100

(c)

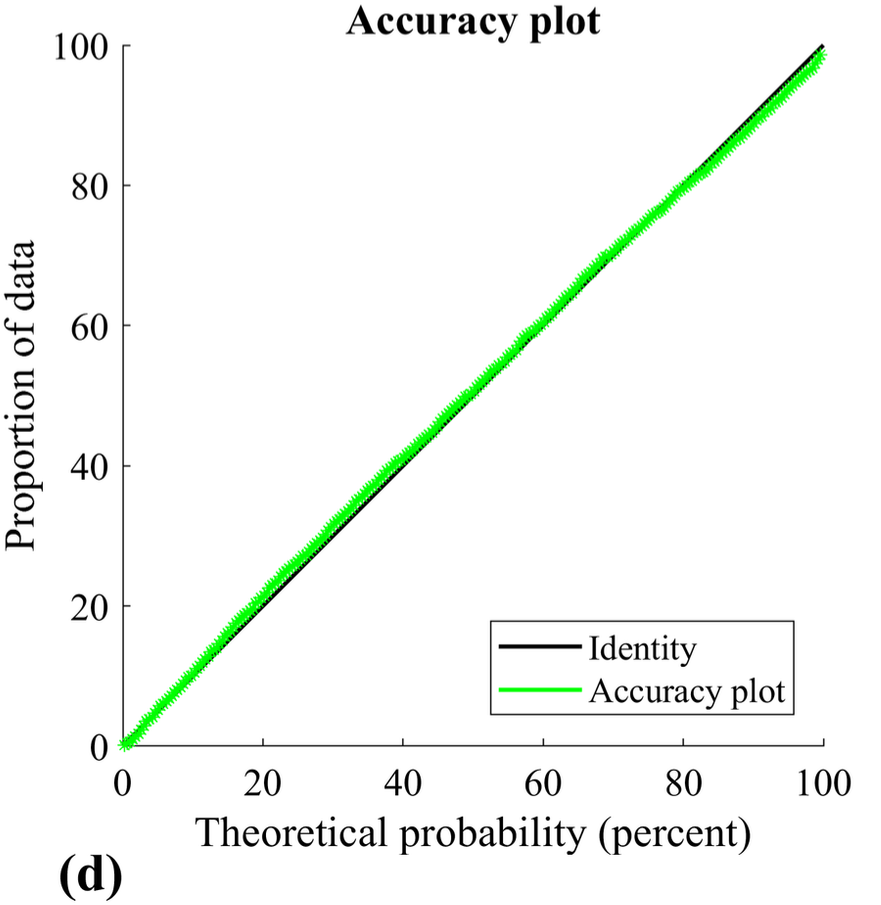
Accuracy plot
Proportion of data
Theoretical probability (percent)
Identity
Accuracy plot
0
20
40
60
80
100

(d)

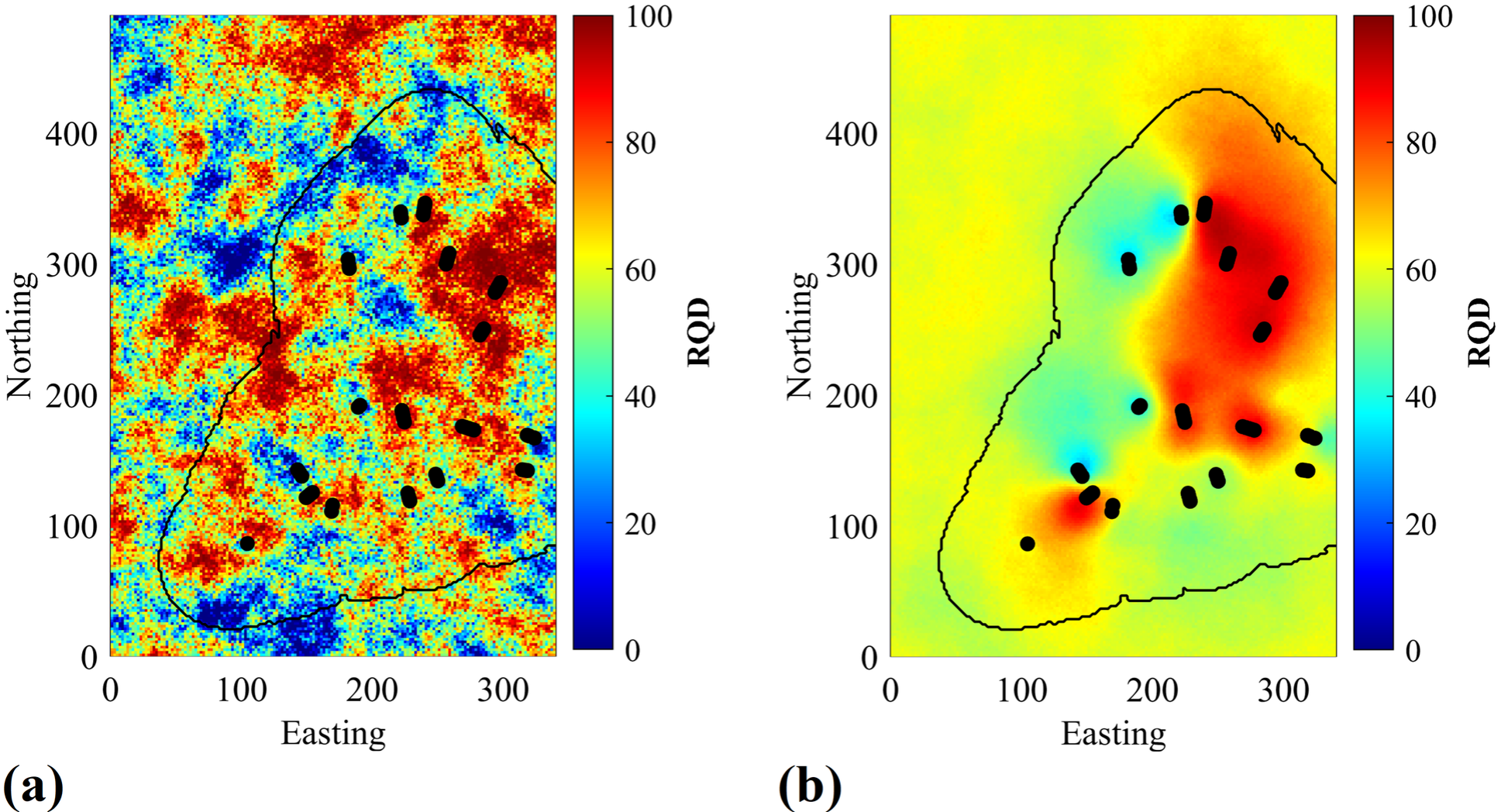
Northing
Easting
RQD
0
100
200
300
400
20
40
60
80
(a)
(b)

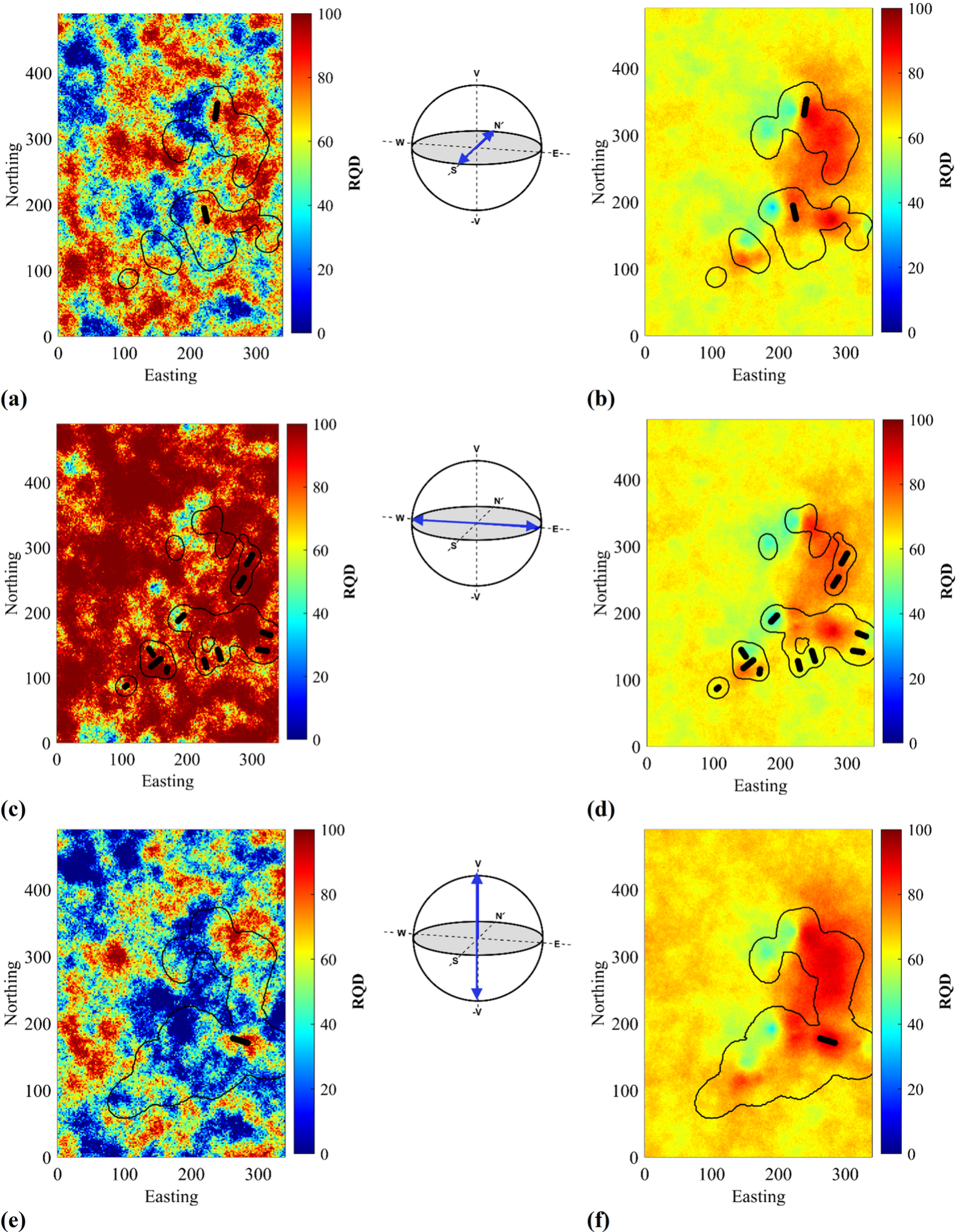
Northing
Easting
RQD
V
-V
N
W
E
S
(a)
(b)
(c)
(d)
(e)
(f)

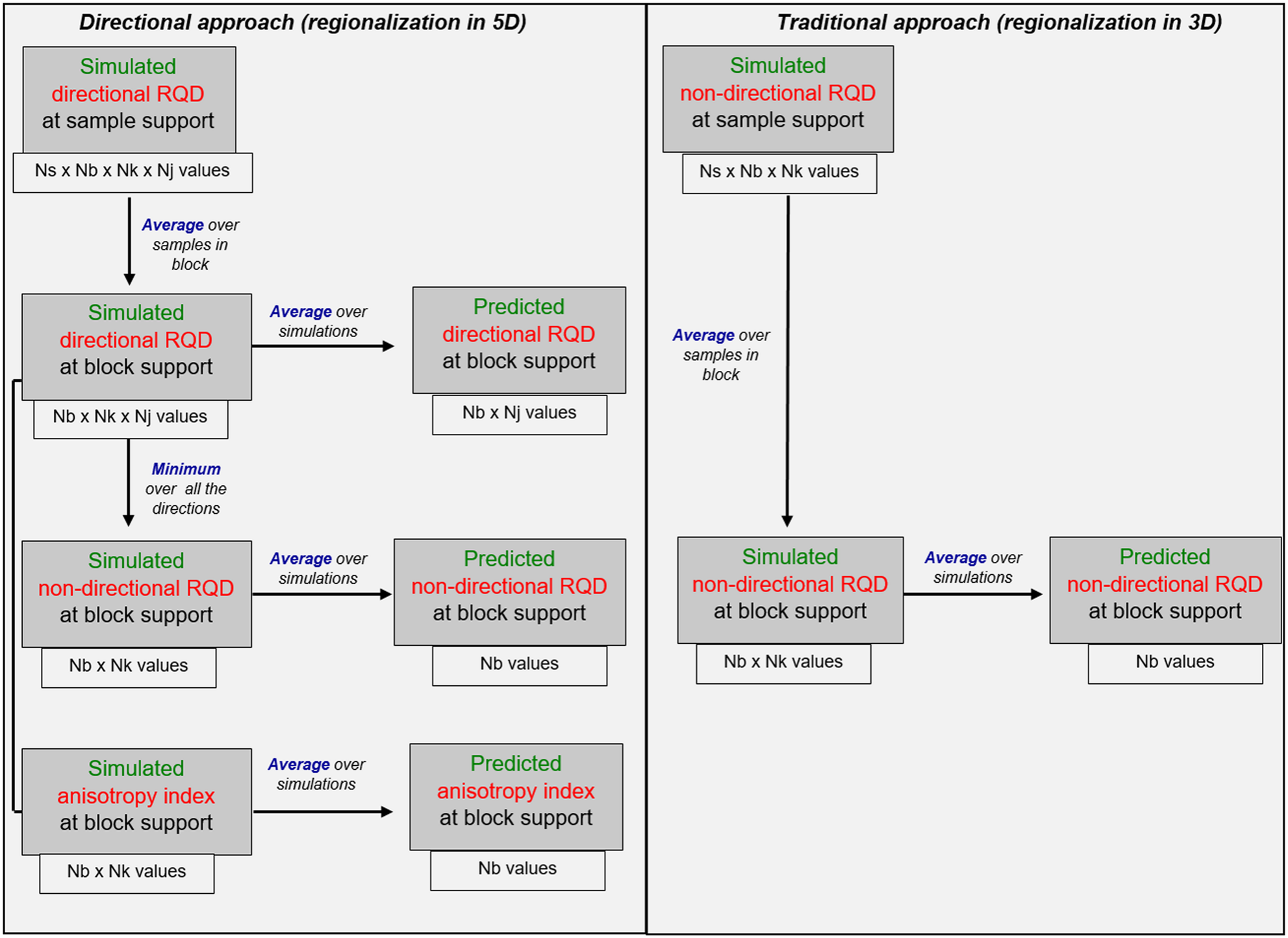
Directional approach (regionalization in 5D)
Simulated directional RQD at sample support
Ns x Nb x Nk x Nj values
Average over samples in block
Simulated directional RQD at block support
Nb x Nk x Nj values
Average over simulations
Predicted directional RQD at block support
Nb x Nj values
Minimum over all the directions
Simulated non-directional RQD at block support
Nb x Nk values
Average over simulations
Predicted non-directional RQD at block support
Nb values
Simulated anisotropy index at block support
Nb x Nk values
Average over simulations
Predicted anisotropy index at block support
Nb values
Traditional approach (regionalization in 3D)
Simulated non-directional RQD at sample support
Ns x Nb x Nk values
Average over samples in block
Simulated non-directional RQD at block support
Nb x Nk values
Average over simulations
Predicted non-directional RQD at block support
Nb values

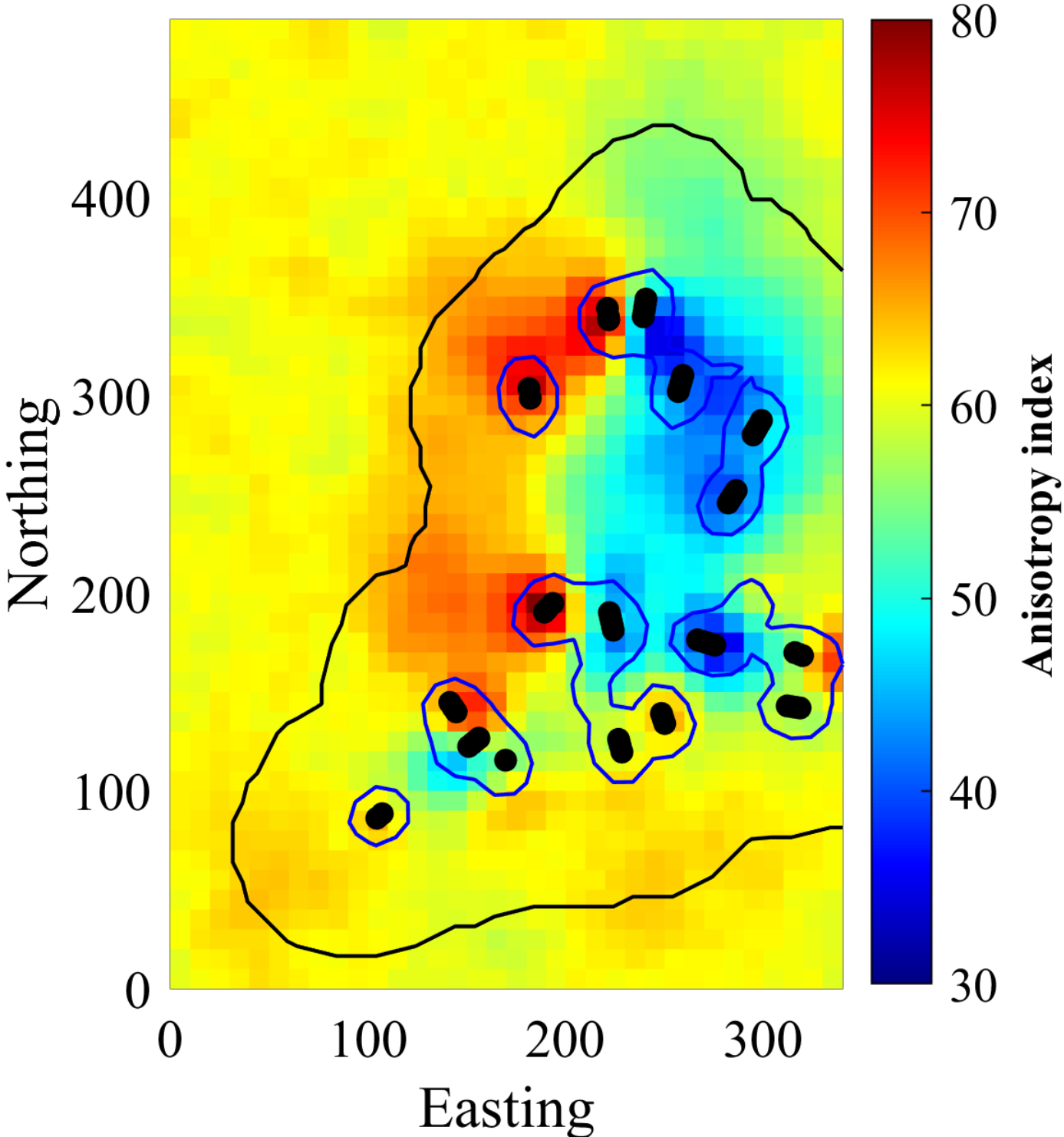
Northing
0
100
200
300
400
0
100
200
300
Easting
80
70
60
50
40
30
Anisotropy index

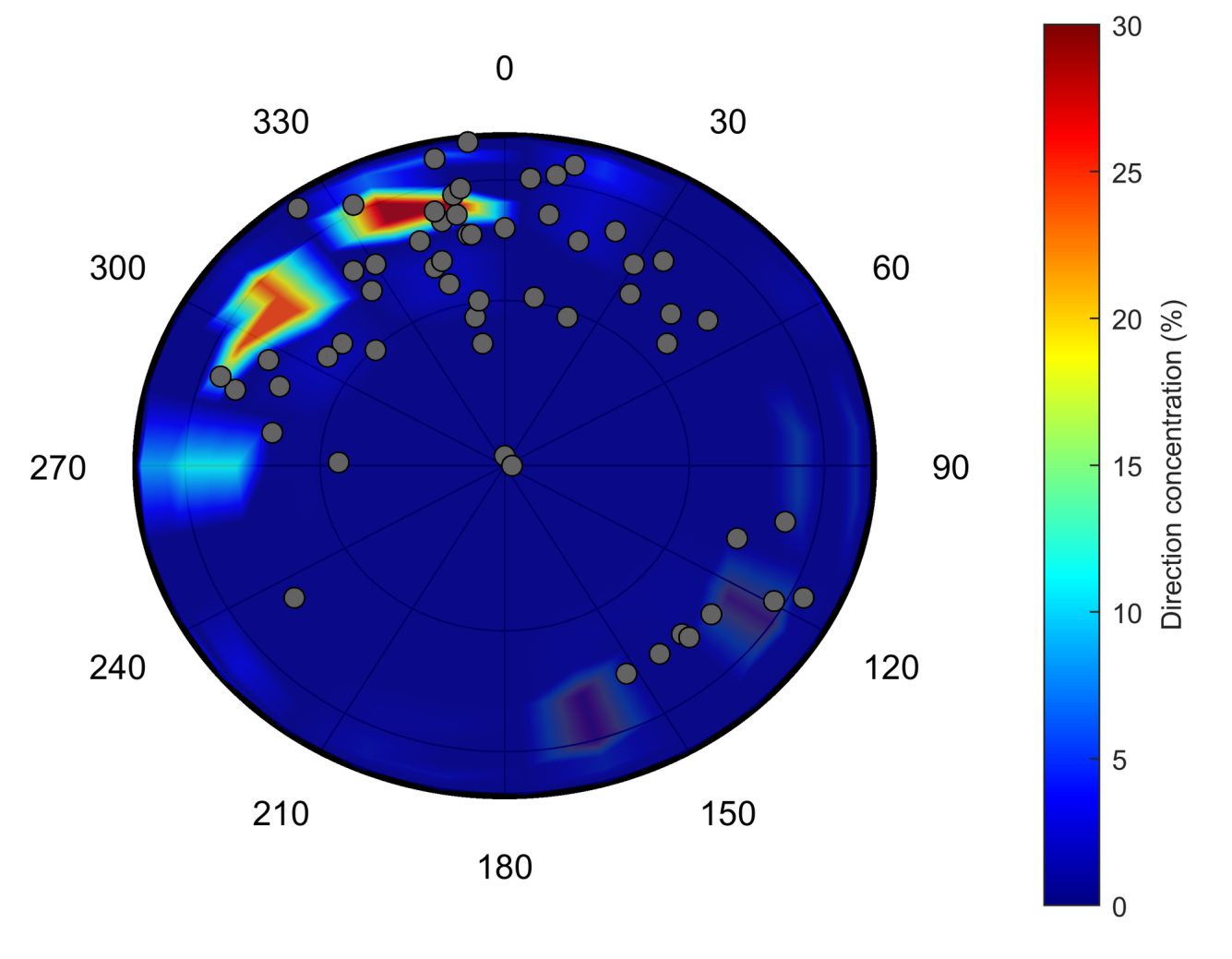
0
30
60
90
120
150
180
210
240
270
300
330
Direction concentration (%)
0
5
10
15
20
25
30

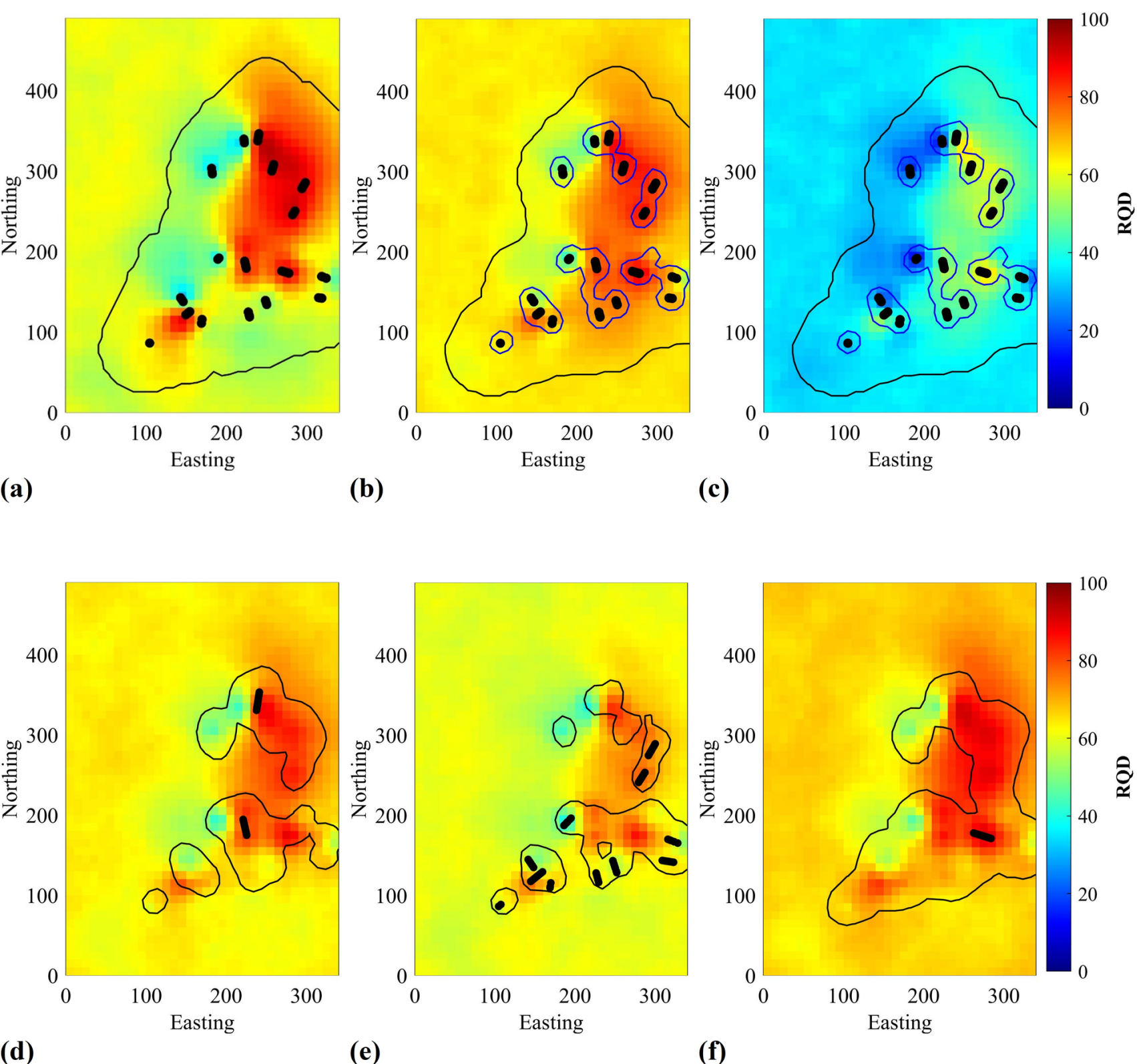
Northing
Easting
RQD
0
100
200
300
400
20
40
60
80
(a)
(b)
(c)
(d)
(e)
(f)

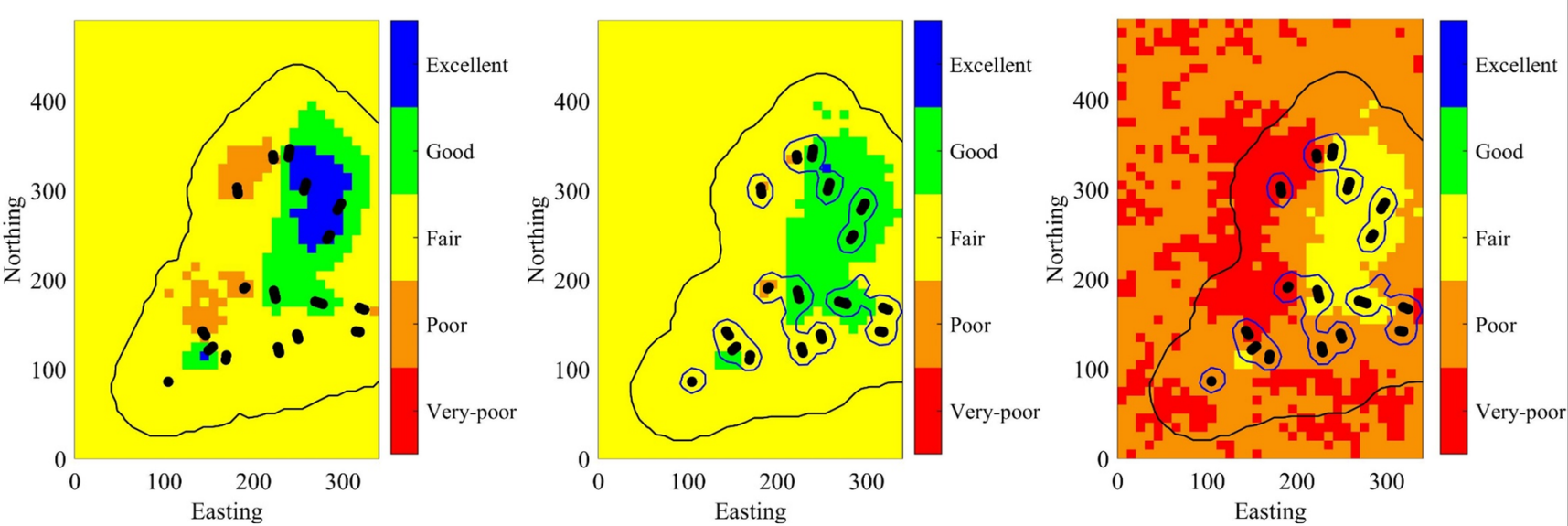
Excellent
Good
Fair
Poor
Very-poor
Northing
Easting
0
100
200
300
400
(a)
(b)
(c)